Received: 30 May 2020 | Revised: 13 January 2021 | Accepted: 16 January 2021

DOI: 10.1002/esp.5079

RESEARCH ARTICLE

ESPL WILEY

On the predictive skill of morphodynamic models for onshore sandbar migration

Viyaktha Hithaishi Hewageegana | Alberto Canestrelli

Department of Civil and Coastal Engineering, University of Florida, Gainesville, FL, USA

Correspondence
Viyaktha Hithaishi Hewageegana, Department of Civil and Coastal Engineering, University of Florida, Gainesville, FL, USA.
Email: vh.hewageegana@ufl.edu

Abstract

A simplified process-based approach for evaluating onshore sandbar migration is presented in this study. This approach takes wave-averaged parameters as input and computes sediment transport processes using a reconstructed intra-wave orbital velocity signal. The proposed method guarantees good predictive skills for multiple onshore sandbar migration cases without an *ad hoc* calibration for each scenario. The study differs from previous onshore sandbar migration models, where calibration and testing are performed on just one or few events, and model assessment for uncalibrated realizations is rarely carried out. The present version of the model only addresses onshore sandbar migrations. For the onshore migration cases analyzed, the model has better predictive skills than state-of-the-art morphodynamic models (XBeach and Unibest-TC).

KEYWORDS
onshore sandbar migration, sediment transport, velocity signal reconstruction, wave asymmetry, wave skewness

1 | INTRODUCTION

Understanding the response of the beach profile and its shallow features (sandbars) in varying wave climates has important implications for a wide range of fields. In particular, after erosive storm events, the gradual onshore migration of sandbars under fair weather conditions favors beach progradation (Dubarbier et al., 2017). Successful prediction of onshore sandbar migration is thus crucial to understand and quantify beach recovery. However, modeling the evolution of sandbars is challenging due to the complex hydrodynamic processes that drive sediment transport and morphological changes. It is understood that offshore sandbar migration is predominantly due to offshore-directed undertow currents during energetic wave conditions (Gallagher et al., 1998; Hsu et al., 2006; Short, 1999; Thornton et al., 1996). Onshore sandbar movements are mostly observed when the incident wave energy is moderate, and wave-averaged mean currents are relatively weak (Hsu et al., 2006; Plant et al., 2004). Several mechanisms are identified as important in onshore sediment transport, which include processes such as boundary layer streaming and the effect of wave shape (Henderson et al., 2004; Nielsen, 2006). As waves shoal in the nearshore, their shape becomes skewed (narrow peaked crests with wide shallower troughs) and asymmetric (wave crest to trough and trough to crest half periods are different). The orbital velocity and acceleration signals also change from sinusoidal to non-sinusoidal form (Abreu et al., 2010; Boechat Albernaz et al., 2019). For progressive waves, when the water level signal is purely skewed, velocities are skewed, and acceleration is symmetrical. On the contrary, when the water level signal is purely asymmetric, velocities are asymmetric, and acceleration is skewed. Accounting for sediment transport due to a non-linear (i.e., non-sinusoidal) wave shape is vital for the accurate prediction of onshore sandbar migration (Hoefel & Elgar, 2003; Hsu et al., 2006).

Wave transformation can be computed using a wave-resolving numerical model (e.g., Jacobsen et al., 2014; Zijlema et al., 2011). However, such models have a high computational cost, restricting their applicability to small temporal and spatial scales. In wave-averaged models, energy fluxes are computed by averaging over the individual waves (Roelvink & Reniers, 2011). While these models run faster, they cannot explicitly solve wave non-linearities. They require parametrizations to account for the effect of wave non-linearities on

sediment transport. Such models' performance on simulating onshore sandbar migrations is insufficient (Fernández-Mora et al., 2015; Wright et al., 1991). For example, the widely used morphodynamic model XBeach shows better performance in erosive states than accretive conditions involving nearshore sandbars (Roelvink & Costas, 2019).

Energetic-type transport models based on moments of the near-bed fluid velocity (e.g., Bailard, 1982; Bowen, 1980) take sediment stirring and transport into account. These approaches resolve the net sediment transport due to velocity skewness. However, for an asymmetric velocity signal with zero velocity skewness, these energetic models will predict no net sediment transport. Experimental observations on asymmetric waves by Nielsen (1992) showed the importance of fluid acceleration on sediment transport. Elgar et al. (2001) analyzed data from the Duck94 field campaign and observed that near the sandbar, under asymmetric waves, water accelerates rapidly, producing high onshore velocities and net onshore sediment transport. To include the effects of wave asymmetry, Drake and Calantoni (2001) proposed a formulation in which sediment transport is a function of fluid acceleration. Using the proposed formula, but neglecting wave skewness, Hoefel and Elgar (2003) were able to model onshore sandbar migration for a single event. Hsu et al. (2006) also modeled shoreward sandbar migration for the same event. However, they only considered sediment transport induced by velocity skewness and neglected the effect of wave asymmetry. Fernández-Mora et al. (2015) further improved the results by considering a combination of acceleration skewness and velocity skewness induced sediment transport to predict onshore sandbar propagation for the same event.

Model approaches proposed in previous studies to predict onshore sandbar migration (e.g., Fernández-Mora et al., 2015; Hajiarabderkani et al., 2017; Hoefel & Elgar, 2003; Hsu et al., 2006; Plant et al., 2004; van Maanen et al., 2008), (i) only employ one (or very few) events to calibrate the model; (ii) use the same event/events to both calibrate model coefficients and to assess the predictive skill of the model. Such a procedure can lead to overfitting of the model and provides no information on the actual prediction skill when the model is applied to forecast uncalibrated scenarios. A notable exception is the studies where onshore and offshore sandbar migrations are modeled at different beaches for multiple sequences of events (e.g., Ruessink et al., 2007).

Here, we propose a model that consists of a coupled hydrodynamic, sediment transport, and morphological modules. Sediment transport is determined by wave acceleration skewness, velocity skewness, wave-averaged mean currents (undertow), and gravity-driven diffusive processes. The model uses an intra-wave near-bottom orbital velocity reconstruction that is estimated using the approach proposed by Elfrink et al. (2006). The orbital velocity reconstruction explicitly resolves the sediment transport driven by wave acceleration skewness and velocity skewness. The current version of the model only addresses onshore sandbar migrations, and offshore migrations are not considered.

Previous studies have presented similar wave-averaged models that account for the effect of intra-wave orbital velocities on sediment transport and onshore sandbar migration (e.g., Dubarbier et al., 2015; Fernández-Mora et al., 2015). The major difference between these models and the model presented in this study is the derivation of coefficients. The proposed model uses a rigorous calibration procedure considering multiple cases to obtain model coefficients. In contrast, previous models use one or a few cases for calibration. Cross-validation is used to calibrate and validate the model's free parameters over a subset of cases. The model performance is then assessed on a testing database not used for calibration. The study uses multiple cases (101) of onshore sandbar migration observed in Duck, NC, for this procedure.

To that extent, this work's primary goal is to propose an approach that guarantees good predictive skills for multiple onshore sandbar migration cases without an *ad hoc* calibration for each scenario and to compare the proposed method with the results from widely used morphodynamic models (XBeach and Unibest-TC). This type of skill assessment and model inter-comparison is lacking in the current literature.

2 | THEORY AND METHODOLOGY

The proposed approach consists of a hydrodynamic module and a morphodynamic module. First, the hydrodynamics is computed, from which sediment transport and bed level changes are calculated.

2.1 | Hydrodynamic module

The hydrodynamic module is depth-averaged, one-dimensional (cross-shore), and assumes a uniform beach in the longshore direction. Wave transformation over the cross-shore is solved from wave energy conservation, which reads:

$$\frac{d}{dx}\left(\frac{1}{8}\rho g H_{\mathrm{rms}}^2 c_{\mathrm{g}} \cos\theta\right) = -D, \tag{1}$$

where x is the cross-shore coordinate, ρ is the density of water, g is gravitational acceleration, H_{rms} is the root-mean-square wave height, c_{g} is the group velocity, θ is the wave angle from shore normal, and D is the wave energy dissipation calculated according to Baldock et al. (1998) as:

$$D = \frac{1}{4T_{\mathrm{p}}}\rho g \exp\left[-\left(\frac{H_{\mathrm{b}}}{H_{\mathrm{rms}}}\right)^2\right]\left(H_{\mathrm{b}}^2 + H_{\mathrm{rms}}^2\right), \tag{2}$$

where T_{p} is the peak wave period and $H_{\mathrm{b}}$is the breaker height. The value of H_{b} is calculated using Battjes and Janssen (1978) as:

$$H_{\mathrm{b}} = \frac{0.88}{k}\tanh\left(\frac{\gamma}{0.88}kh\right), \tag{3}$$

where k is the wavenumber, h is the water depth (including the tide level), and γ is a calibration coefficient. From field measurements

(including data from Duck, NC), Ruessink et al. (2003) found the following expression for γ:

$$\gamma = 0.76kh + 0.29. \quad (4)$$

Wave refraction is computed using Snell's law:

$$k_1 \sin\theta_1 = k_2 \sin\theta_2, \quad (5)$$

where the subscripts 1 and 2 denote two locations along the cross-shore.

The depth-averaged undertow current (U_x) is calculated from the Stokes drift using mass conservation (Brown et al., 2015), and it reads:

$$U_x = \frac{-\omega H_{rms}^2 \cos\theta}{8h \tanh(kh)}, \quad (6)$$

where ω is the radial frequency.

Elfrink et al. (2006) proposed a method to reconstruct the intra-wave near-bottom orbital velocity signal (U_{orb}). The formulae are generated from evolutionary algorithms developed using a large amount of measured wave, velocity, and morphological data from different field observation sites (including Duck, NC). The near-bed orbital velocity signal is generated using wave height, wave period, water depth, and local bed slope. Their method was successful in accurately reconstructing observed velocity signals. Figure 1 illustrates an example of near-bed orbital velocity reconstruction for a given boundary wave condition.

2.2 | Sediment transport and morphological module

Sediment mobility in oscillatory flows is affected by time-history effects, delayed response of sediments, and turbulent burstings (Ribberink, 1998; Ribberink & Al-Salem, 1994). Hence, the calculation of sediment transport due to waves is challenging. Processes can be simplified by assuming a quasi-steady approach to calculate the instantaneous bed shear stress and subsequent sediment transport (Hsu et al., 2006; Traykovski et al., 1999). The quasi-steady bed shear stress can be substituted into Mayer–Peter–Muller power-law resulting in an energetic type sediment transport formula, which is

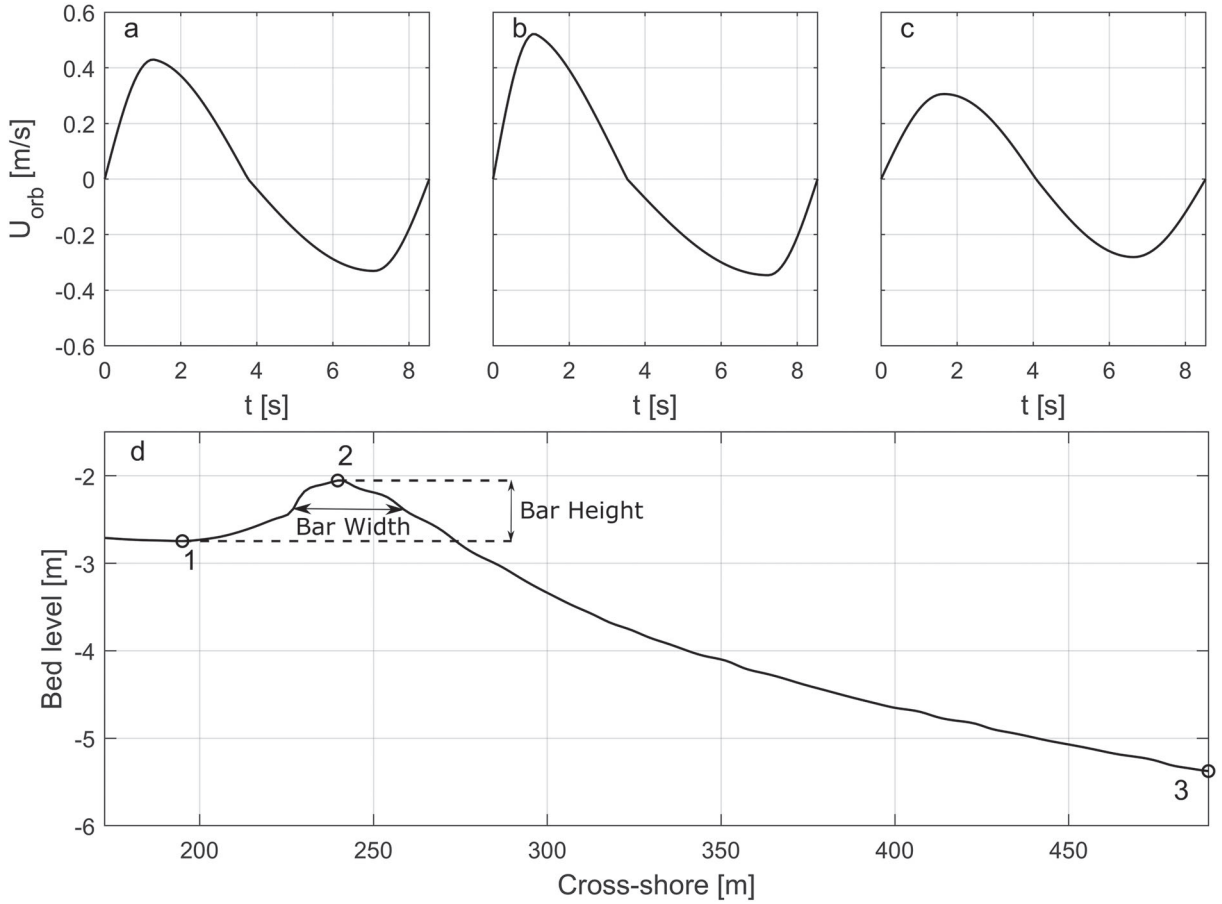

FIGURE 1 Example of near-bed orbital velocity reconstruction at three locations for boundary wave condition H_{rms} = 0.42 m, T = 8.5 s. (a–c) Near bed orbital velocity signal at locations 1–3, respectively. (d) The bed level in cross-shore direction. Sandbar height is defined as the vertical distance between the sandbar crest and the landward trough. Sandbar width is defined as the horizontal distance between the landward and seaward bed locations on either side of the crest at half sandbar height

based on the moments of flow velocity (Hsu et al., 2006). Such formulae are able to capture the sediment transport due to skewness in the velocity signal. Net sediment transport due to velocity skewness (S_{vsk}) and mean currents (S_c) over a wave cycle are thus determined using velocity moments (Hsu et al., 2006):

$$S_{vsk} = \frac{k_v}{(s-1)g}\left(\frac{\varepsilon_B}{\tan(\phi)} < |U_{orb}|^2 U_{orb} > + \frac{\varepsilon_S}{W_o} < |U_{orb}|^3 U_{orb} >\right), \quad (7)$$

$$S_c = \frac{k_c}{(s-1)g}\left(\frac{\varepsilon_B}{\tan(\phi)} < |U_{orb}|^2 > U_x + \frac{\varepsilon_S}{W_o} < |U_{orb}|^3 > U_x\right), \quad (8)$$

where k_v[−] and k_c[−] are calibration coefficients, U_{orb} is the intra-wave orbital velocity vector, ε_B and ε_S are transport efficiency factors, ϕ is the friction angle, s = 2.65 is the specific gravity, and W_o is the sediment fall velocity, taken as 0.025 m s^{-1}. The fall velocity was calculated for a median grain size of 0.2 mm, which was taken as the representative value for Duck, NC, where the median gain size varied from 0.3 mm at the shoreline to 0.15 mm offshore (Hoefel & Elgar, 2003). The angle brackets denote time averaging. The values of ε_B and ε_S are set to 0.135 and 0.015, respectively, and tan(ϕ) is set as 0.63 (Fernández-Mora et al., 2015; Gallagher et al., 1998).

For a purely asymmetric wave, Equation 7 would predict zero net sediment transport. However, skewed pressure gradient forces acting on the sediments result in a net sediment transport (Hallermeier, 1982; Watanabe & Sato, 2005). The effect of pressure gradient on sediments can be estimated using the flow acceleration (Nielsen, 2006). One practical method of evaluating the acceleration related sediment transport is through the acceleration skewness (a_{spike}) of the flow. The acceleration skewness (which is a measure of velocity asymmetry) induced sediment transport (S_{ask}) is determined according to Drake and Calantoni (2001) as:

$$S_{ask} = \begin{cases} k_a\left(a_{spike} - \text{sign}\left(a_{spike}\right)a_{cr}\right) & \text{for } |a_{spike}| \geq a_{cr} \\ 0 & \text{for } |a_{spike}| < a_{cr} \end{cases}, \quad (9)$$

where k_a,of units milliseconds, is a calibration coefficient, a_{cr} is the threshold that needs to be exceeded to initiate sediment transport due to acceleration skewness, which has been set to 0.2 m s^{-2} (Hoefel & Elgar, 2003). The a_{spike} is defined as a_{spike} = $< a^3 > / < a^2 >$ where a is the acceleration time series.

Diffusive sediment transport due to gravity (S_D) is represented as in Fernández-Mora et al. (2015):

$$S_D = \frac{k_d}{\rho}\left[\frac{E_w}{\frac{dz_b}{dx} - \tan\phi}\right]\left(\frac{\frac{dz_b}{dx}}{\tan\phi}\right), \quad (10)$$

where k_d, of units s m^{-1}, is a calibration coefficient, E_W is the wave energy density, and $\frac{dz_b}{dx}$ is the bottom slope. The total sediment transport rate is calculated as the combined transport due to acceleration skewness, velocity skewness, mean currents, and diffusion, which read:

$$S_{tot} = S_{ask} + S_{vsk} + S_c + S_D. \quad (11)$$

The bed elevation is updated using sediment mass conservation (usually known as the Exner equation):

$$\frac{dz_b}{dt} = \frac{1}{(1-p)}\frac{dS_{tot}}{dx}, \quad (12)$$

where z_b is the bed level, t is time, and p is the porosity of sediment (set to 0.3).

2.3 | Boundary conditions, numerical implementation and model setup

Tide is prescribed as a time-varying instant water level across the whole domain. Hence, no tide-induced current resulting from the change in the tidal level is calculated. The measured wave parameters set the offshore boundary condition of the hydrodynamic module. The offshore wave-height is transformed over the cross-shore using Equations 1–5. The calculation is performed on a uniformly spaced grid in the cross-shore direction using an Euler-explicit finite differencing method. The transformed wave height is used to calculate the intra-wave orbital velocity signal and wave-averaged current. The calculated velocities are then incorporated to find the sediment transport fluxes using Equations 7–10.

The sediment fluxes are defined at the interfaces of a staggered grid. The offshore boundary condition (right boundary) for sediment flux is set to a Neumann type (zero gradient). In the nearshore boundary (left boundary), the sediment transport in the leftmost interface is set to the transport flux calculated at the leftmost cell center (transmissive boundary condition).

Finally, the bed level change due to the sediment fluxes is calculated by Equation 12 using an Euler-explicit finite-difference method. The updated bed level is then looped back to estimate the wave hydrodynamics in the next time step.

2.4 | Bottom profiles and hydrodynamic data

Researchers at the Field Research Facility (FRF) in Duck, NC have been collecting hydrodynamic and morphological data over the past four decades. Cross-shore beach transects and hydrodynamic data (i.e., wave height, wave period, wave direction, and water level) collected between January 1990 and July 2019 are used in this study.

In this work, we searched for pairs of sequential profile surveys in which a sandbar is present, and it moves onshore. The sandbars were identified using local maxima and minima in the bed profiles. Note that this approach does not identify the sandbars in the swash zone, as they are diffused over the swash zone and do not usually show clear maxima or minima. Sandbar height was defined as the vertical distance between the sandbar crest and the landward trough (Figure 1d). Sandbar width was defined as the horizontal distance

between the landward and seaward bed locations on either side of the crest at half sandbar height (Figure 1d). Thresholds were considered on the sandbar height (sandbar height > 0.1 m) and width (sandbar width > 10 m) to filter out the identification of small perturbations in the bed as sandbars. The migration of a sandbar was classified as onshore if the current sandbar crest was located shoreward of the previous crest location. We only retained the cases in which a single sandbar was present. Since the model assumes longshore uniformity and does not include longshore processes, pairs of cross-shore profiles for which bottom changes were likely influenced by gradients in longshore sediment transport were removed. To this aim, mass conservation was used, and pairs of profiles with mass changes larger than ±25% were removed. After the filtering, a set of 101 cases were selected for the study.

The offshore wave parameters (wave height, wave period, and wave direction) for each case were obtained from the wave data collected at 8 m water depth. The water levels were gathered from the tide station situated at the FRF pier. Figure 2 summarizes event duration, wave climate, and the observed onshore displacement of the cases used in the study. The cumulative energy flux for each event was calculated according to Vidal-Ruiz and Ruiz de Alegría-Arzaburu (2020). The tidal signal at Duck, NC is semidiurnal with an amplitude of 0.5 m (Figure 3d).

Using long-term measurements, Vidal-Ruiz and Ruiz de Alegría-Arzaburu (2019, 2020) identified different modes of onshore sandbar migrations (modes I–IV) based on the cumulative wave energy and sandbar morphometric properties. The onshore sandbar migration cases used in the current study can be generally classified under mode I, where the sandbar is moving onshore under low-energetic conditions (< 50 kW m^{-1}) and subsequently weld with the shoreline.

Figure 3 presents an example of an onshore sandbar migration event (case 05) and the corresponding time series of wave height, period, direction, and tidal level observed during the migration period.

2.5 | Model training

To predict sandbar migration, the model needs to be trained to obtain the optimal calibration coefficients associated with the sediment transport processes, that is k_a,k_v, k_c, and k_d in Equations 7–10. Brier skill score (BSS) is extensively used as a parameter to calibrate model coefficients and measure the model skill (Ruessink, 2005; Splinter et al., 2011; Vousdoukas et al., 2012; Simmons et al., 2017). BSS reads:

$$\mathrm{BSS} = 1 - \frac{< \left(z_{b,\mathrm{model}} - z_{b,\mathrm{obs}_{fin}}\right)^2 >}{< \left(z_{b,\mathrm{obs}_{fin}} - z_{b,\mathrm{obs}_{init}}\right)^2 >}, \tag{13}$$

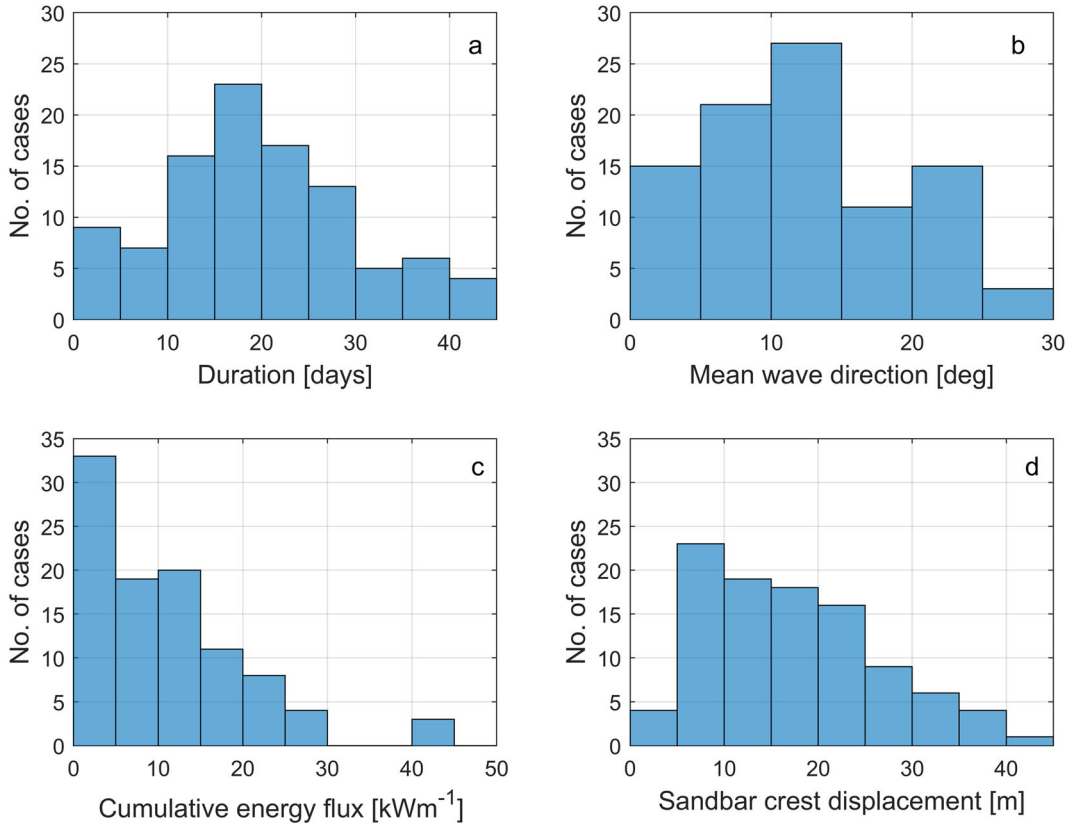

FIGURE 2 Duration, wave conditions, and observed sandbar displacement for the cases considered in the study. (a) The time duration between initial and final bed measurements, (b) mean offshore wave direction with respect to the shore normal, (c) cumulative energy flux, and (d) sandbar crest displacement

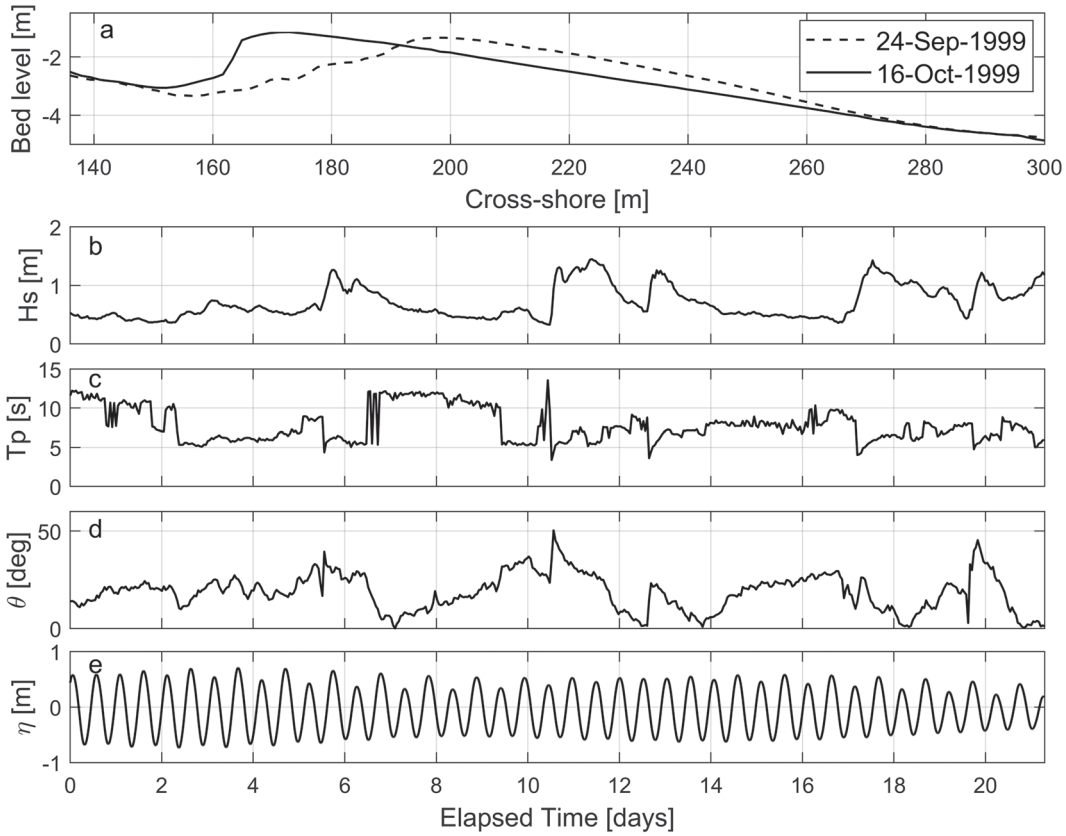

FIGURE 3 Wave climate and consequent bed level change for case 05. (a) Initial and final measured bed level. The cross-shore distance is measured from the shoreline. Time series of (b) significant wave height (H_s), (c) peak wave period (T_p), (d) wave direction from shore normal (θ), and (e) water level (η)

where $z_{b,model}$ is the bed elevation predicted by the model, $z_{b,obs_{fin}}$ is the measured final bed elevation and $z_{b,obs_{init}}$ is the measured initial bed elevation. The angle brackets denote averaging over the profile section under consideration. Since the study explicitly focuses on the sandbar evolution, the BSS is computed from the onshore sandbar trough (location 01 in Figure 1d) to 250 m offshore of the sandbar crest (location 03 in Figure 1d), both referenced to the measured final profile. The BSS values can be used to interpret the model predictive capability as follows: no model skill (BSS < 0), poor model skill (0.0–0.3), fair model skill (0.3–0.6), good model skill (0.6–0.8), and excellent model skill for BSS > 0.8 (Splinter et al., 2014; van Rijn et al., 2003).

A subset of all cases was randomly selected as training cases and was used to calibrate the model. An objective function J is defined to measure the model capability in predicting the sandbar morphology compared to the measurements, which reads:

$$J(k_a,k_v,k_c,k_d) = \frac{\sum_{i=1}^{N}(1-\mathrm{BSS}(i))^2}{N}, \quad (14)$$

where N is the number of cases in the training data. A lower J indicates that, on average, the modeled sandbar morphology is close to the measured bed for all cases considered. The optimization procedure uses the Nelder–Mead simplex algorithm (Lagarias et al., 1998) to obtain the coefficients that minimize J (Equation 14). The model parameters were initialized for the optimization process using the coefficients obtained by similar studies (e.g., Fernández-Mora et al., 2015; Hoefel & Elgar, 2003; Hsu et al., 2006).

2.6 | Division of data into training, validation, and testing

A cross-validation scheme was implemented to select the optimum coefficients and evaluate the robustness of the proposed model. A set of 80 cases was randomly selected from the total 101 cases as training data, and the rest (21 cases) were partitioned off as test data.

A K-fold cross-validation scheme was used on the data. The total training data (80 cases) were randomly binned into K = 4 equal folds (20 cases in each). From the four folds, three were retained as validation data for testing the model, and the remaining fold was used as training data. The cross-validation process was then repeated four times, with each of the K fold used once as the training dataset to find the optimal sediment transport coefficients (k_a,k_v,k_c,k_d) by minimizing the objective function (Equation 14). Note that in a typical cross-

validation procedure, the training dataset is larger than the validation dataset. However, performing the optimization over many cases carries a high computational cost, since the morphodynamic model has to run for each case and multiple times, till convergence. For this reason, one fold was used for model training, and the remaining three folds for validation.

3 | RESULTS

3.1 | Model training with cross-validation

Figure 4 shows the optimal coefficients when optimization is performed over a batch consisting of an entire fold (Equation 14 with N=20, i.e., batch optimization) and when the optimization is performed for every single case separately (Equation 14 with N=1, hereinafter named "individual optimization"). Individual optimization will be discussed later, and here only batch optimization is discussed. Some cases (case 18 in Fold 2, cases 19 and 58 in Fold 3, cases 45 and 68 in Fold 4) perform poorly (BSS ≤ 0.3) when the coefficients from batch optimization are used in the model. Table 1 provides the coefficients obtained for each fold. Note that the obtained values for each of the coefficients have the same order of magnitude over the different folds.

For each K-fold, the trained coefficients were used in the model to compute the morphodynamic evolution of the sandbar for the correspondent validation set (60 cases). Figure 5 illustrates the BSS results obtained for each validation set. For all validation sets, over 65% of the cases resulted in a BSS > 0.6, while only less than 1% of the cases have a no-skill/poor model skill (BSS < 0.3). Some cases

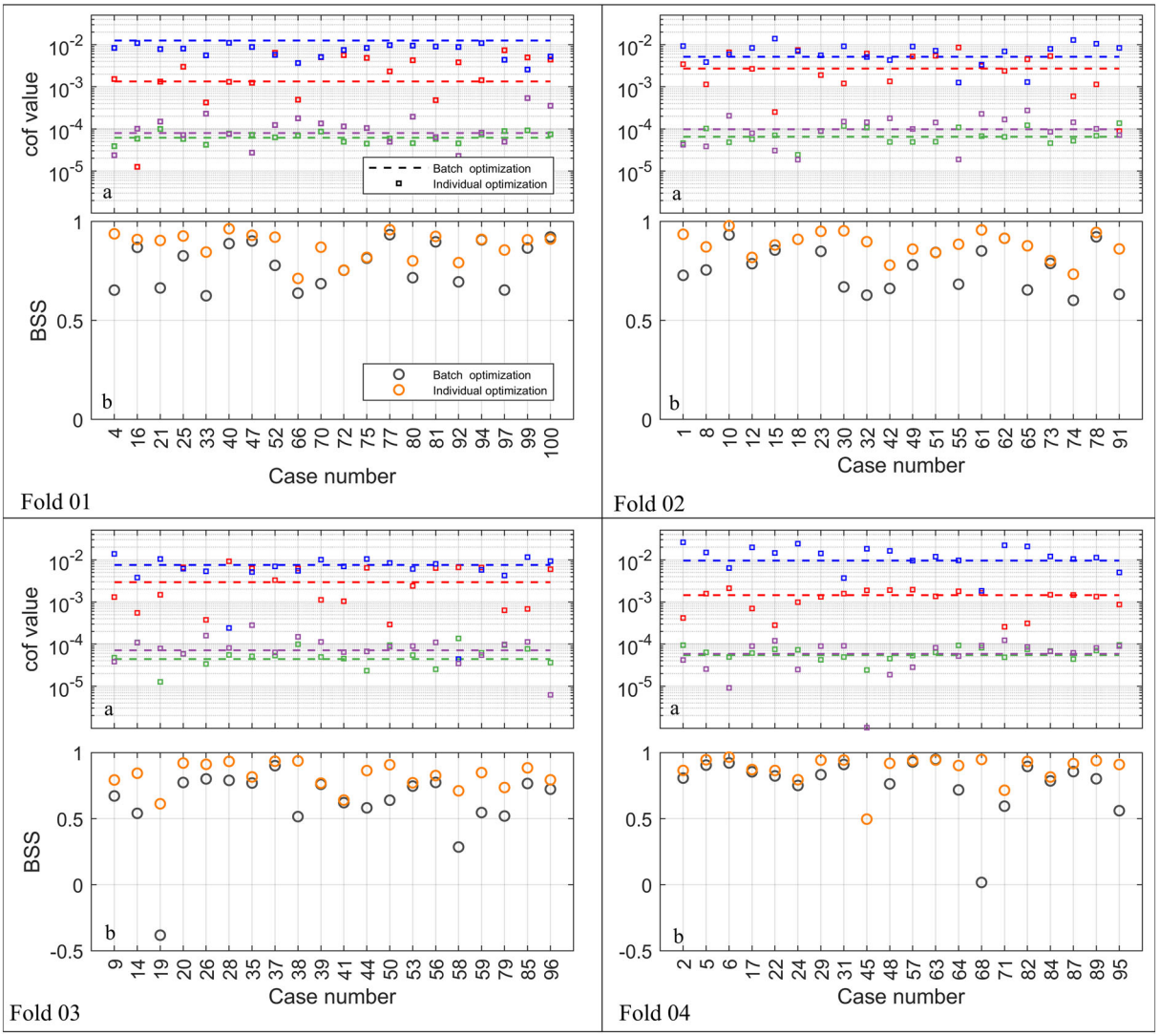

FIGURE 4 Trained coefficients and BSS values for the four folds (Folds 1–4) using batch optimization and individual optimization. (a) The green, red, blue, and purple dashed lines refer to the batch-optimized k_a, k_v, k_c and k_d values, respectively. The green, red, blue, and purple squares indicate individually optimized k_a, k_v, k_c and k_d values, respectively. (b) The black and orange dots refer to BSS values obtained for each model using the batch optimized coefficients and individually optimized coefficients, respectively

TABLE 1 Trained sediment transport coefficients from batch optimization for each *K*-fold in Figure 4

	k_a	k_v	k_c	k_d	Average Brier skill score ($\overline{BSS}$)
Fold 1	6.16×10^{-5}	1.34×10^{-3}	12.54×10^{-3}	7.98×10^{-5}	0.78
Fold 2	6.51×10^{-5}	2.71×10^{-3}	5.17×10^{-3}	9.83×10^{-5}	0.70
Fold 3	4.40×10^{-5}	2.95×10^{-3}	7.57×10^{-3}	7.11×10^{-5}	0.62
Fold 4	5.46×10^{-5}	1.45×10^{-3}	9.61×10^{-3}	5.85×10^{-5}	0.63

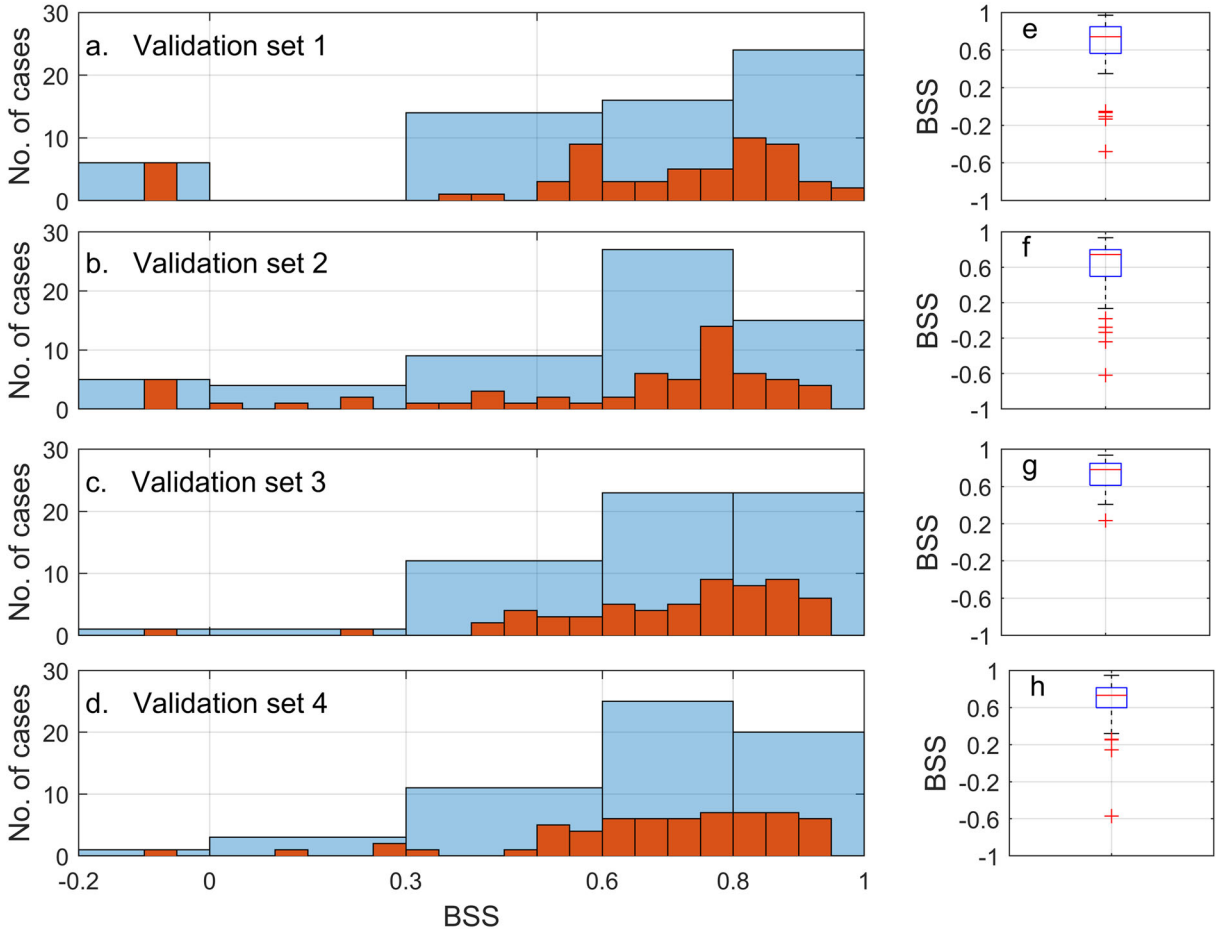

FIGURE 5 (a–d) BSS results for the 60 validation cases corresponding to each "*K*" fold. Blue bins represent the BSS classification: no-skill, poor, fair, good, and excellent. The red bins provide the BSS at a high bin resolution of 0.05. (e–h) Box and whisker plots for BSS values for the k^{th} validation dataset. Outliers are defined as values greater than or less than Q_3+1.5 × IQR,Q_1 − 1.5 × IQR where $Q_1$and Q_3 are the first and third quartile of the data, respectively, and IQR is the interquartile range

resulted in BSS < 0. These BSS results are lumped to BSS = − 0.1 in the histogram of Figure 5 for effective representation. The cases in which BSS < 0 have values spanning from −0.5 to −0.1 for the validation set 1 (Folds 2, 3, and 4) and from −0.6 to −0.1 for the validation set 2 (Folds 1, 3, and 4). Only a single negative BSS case was found for the validation sets 3 and 4 (Folds 1, 2, 4 and Folds 1, 2, 3, respectively), which had a BSS of −2.2 and −0.57, respectively. The results are comparable and consistent over the four validation sets and show similar skill. Hence, it demonstrates that the model coefficients are not overfitting a specific set during the training process.

3.2 | Model testing

Coefficients derived from training Fold 4 ($k_a = 5.46 \times 10^{-5}$, $k_v = 1.45 \times 10^{-3}$, $k_c = 9.61 \times 10^{-3}$, $k_d = 5.85 \times 10^{-5}$) were chosen as the parameter values of the model. The selected sediment transport coefficients were then used to compute the morphodynamic evolution of the sandbar for the remaining test set (21 cases). Bed levels predicted for nine test profiles (three from each of the excellent, good, and fair categories) are shown in Figure 6.

Figure 7 presents the BSS results for the test dataset. The average BSS for the test cases is 0.64, and the standard deviation is 0.19.

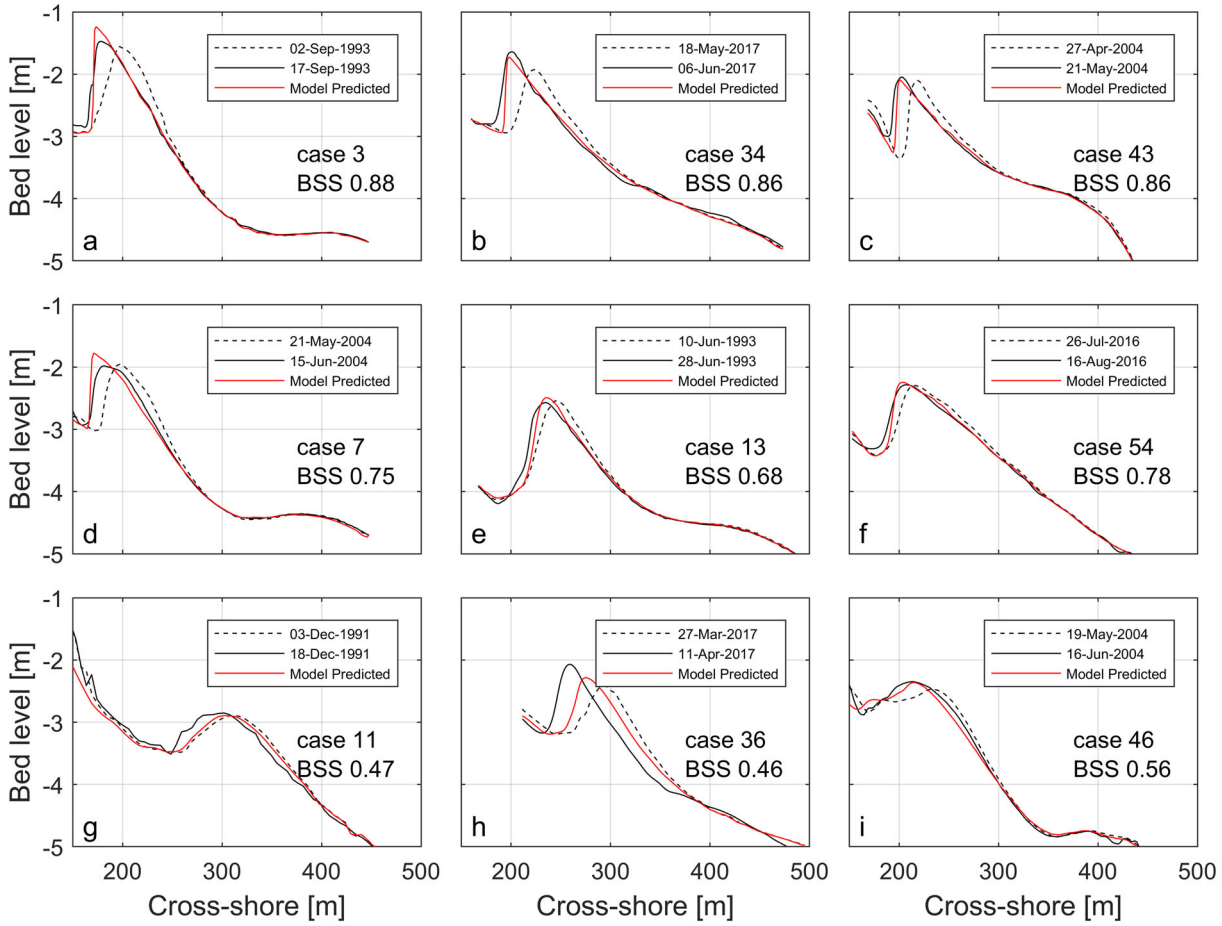

FIGURE 6 The model predicted sandbar morphology for nine test cases, falling under excellent (a–c), good (d–f), and fair (g–i) skill categories. The black dashed line refers to the observed initial bed level. The black and red solid lines indicate the final observed and modeled bed level, respectively. The cross-shore distance is measured from the shoreline

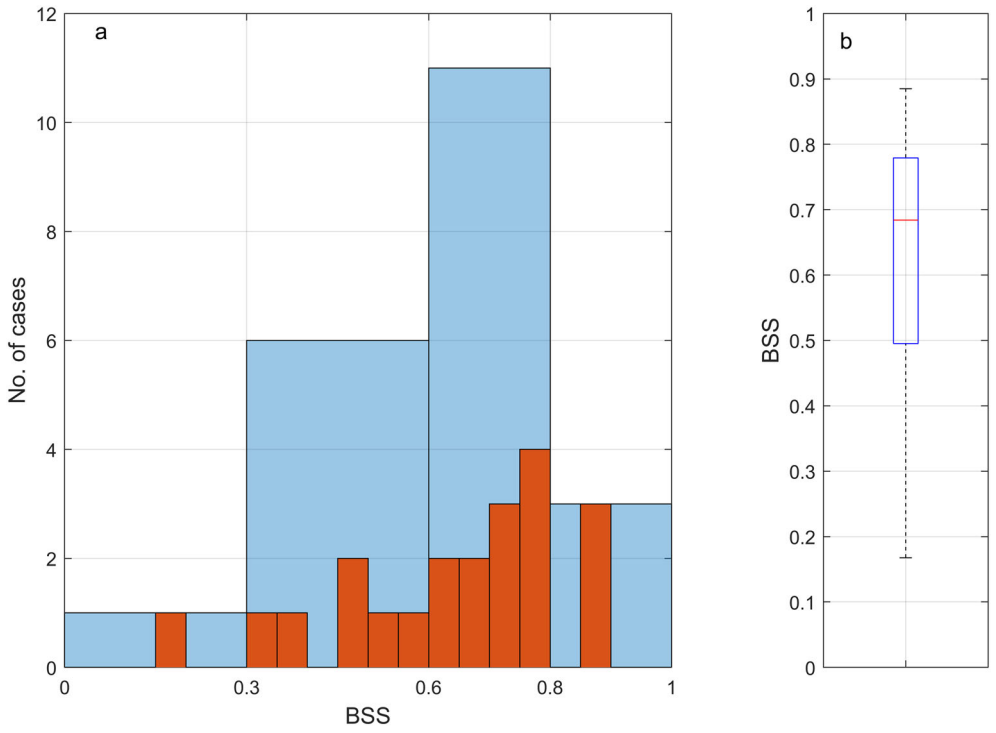

FIGURE 7 (a) BSS results for the test dataset. Blue bins represent the BSS classification: poor, fair, good, and excellent. The red bins provide the BSS at a bin resolution of 0.05. (b) Box and whisker plots for BSS values for test cases

Fourteen out of the total 21 cases can be classified as having good/excellent model skill, while only two cases have a poor model skill.

3.3 | Morphometric comparison

The model's ability to predict morphometric quantities, such as sandbar width, height, and crest migration, were assessed. The model results are obtained using the coefficients derived earlier ($k_a = 5.46 \times 10^{-5}$, $k_v = 1.45 \times 10^{-3}$, $k_c = 9.61 \times 10^{-3}$, $k_d = 5.85 \times 10^{-5}$). To provide an overall assessment of predictive skill, model results for all 101 cases are considered (i.e., 20 cases used in training and the 81 cases used in validation and testing). The results for all the 101 cases are presented in Figure 8. The BSS results (Figure 8d) show that 74% of the cases have a good or excellent model score (BSS > 0.6), while only 7% of the cases have a poor model skill (BSS < 0.3). Two cases resulted in BSS of −0.57 (case 19) and −2.0 (case 45). These are lumped in the histogram in Figure 8 as BSS = − 0.1 for ease of representation. The average Brier Skill Score ($\bar{BSS}$) for all cases was 0.66 and the standard deviation was 0.35.

Figure 8(a–c) illustrates the comparison between modeled sandbar height, width, and crest displacement with the corresponding measured values. The presented approach can simulate the sandbar height and width satisfactorily (mean absolute error on sandbar height and width is 0.16 m and 5.5 m, respectively). The model can also simulate the change in the location of the sandbar in the cross-shore direction (mean absolute error on the movement of the sandbar is 8.6 m).

4 | DISCUSSION

4.1 | Contribution of sediment transport processes in sandbar movement

The presented model contains four sediment transport processes: sediment transport due to acceleration skewness (S_{ask}), velocity skewness (S_{vsk}), wave averaged (undertow) currents (S_c), and diffusive transport due to gravity (S_D). Figure 9(a) illustrates the average sediment transport of each process for case 02. The corresponding bed level change is presented in Figure 9(b). The S_{vsk} is more significant in the wave-shoaling zone compared to S_{ask}. In the nearshore, wave asymmetry dominates over skewness. Therefore, higher transport from acceleration skewness is observed compared to S_{vsk}. Both S_{ask} and S_{vsk} show a maximum over the sandbar and wane as waves lose energy. The wave-averaged currents (undertow) results in an

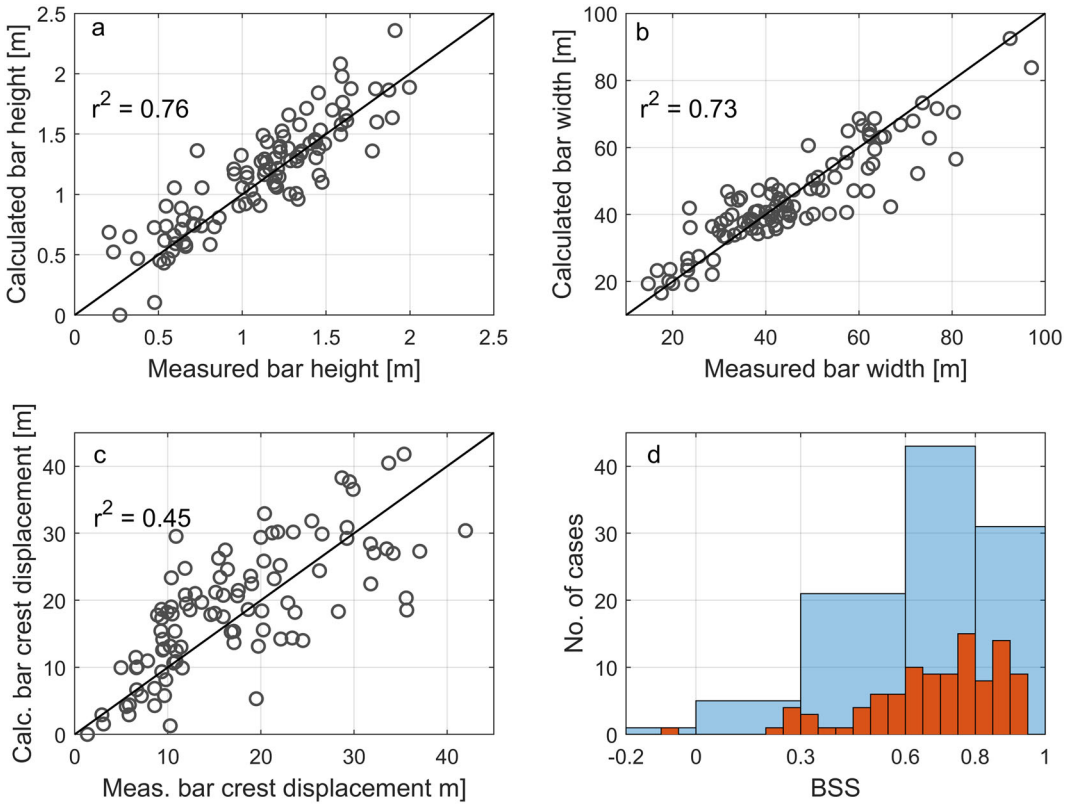

FIGURE 8 Comparison between measured and predicted (a) sandbar height, (b) width, and (c) sandbar crest displacement for all cases. The r^2provides the correlation between the measured and the predicted values. (d) BSS results for all cases. Blue bins represent the BSS classification: no-skill, poor, fair, good, and excellent. The red bins provide the BSS at a bin resolution of 0.05

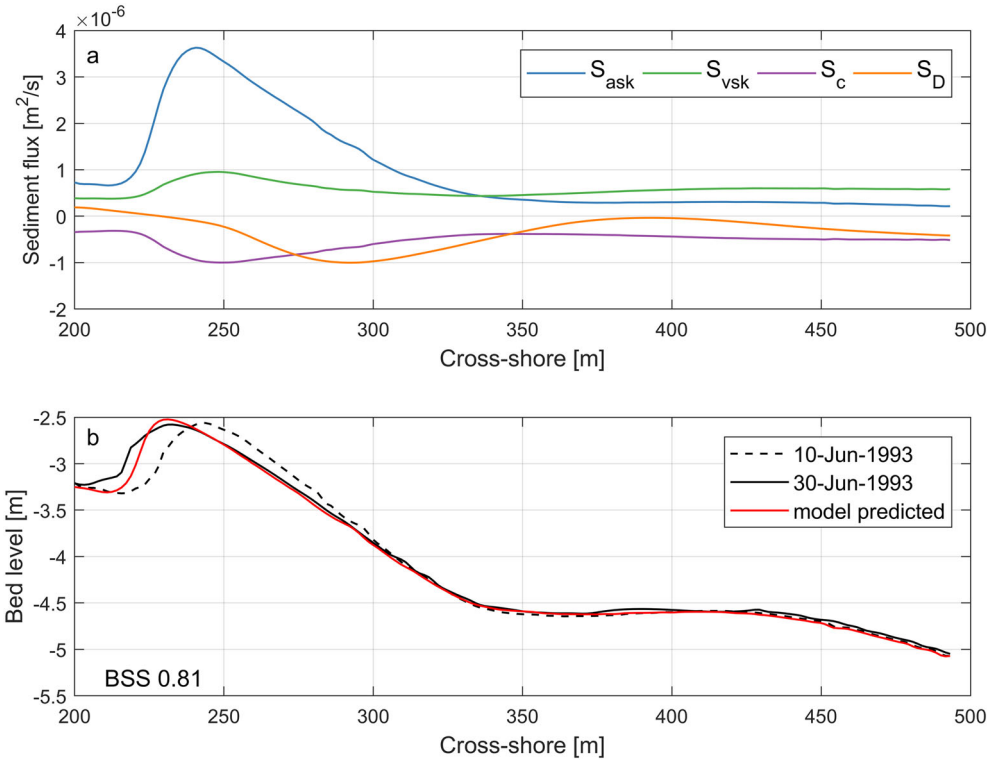

FIGURE 9 Average sediment transport fluxes for case 02 ($\bar{H}_s = 0.58\,m, \bar{T}_p = 8.6\,s$). (a) Calculated average sediment transport rates for the four transport processes over the bar. (b) Bed profile over the cross-shore. The black dashed line refers to the observed initial bed level. The black and red solid lines indicate the observed final and model predicted bed level, respectively. The cross-shore distance is measured from the shoreline

offshore-directed transport and is maximized over the sandbar crest. Gravity-driven diffusive transport (S_D) moves sediments depending on the bed slope. Thus, S_D changes direction over the sandbar crest.

The present modeling scheme is based on the free-stream velocity and acceleration. It has been found that significant changes occur to the flow near the bed that influence the sediment transport processes (e.g., Henderson et al., 2004; Henriquez et al., 2014). However, bedload transport computed using the proposed model was able to estimate the observed bedload transport in flume experiments with reasonable accuracy (section 4.4).

Transport gradients lead to bed accretion and erosion. Figure 10 illustrates bed level changes over the sandbar as a function of time for the same event described in Figure 9 (case 02). Acceleration and velocity skewness carry sediments onshore and deposit them on the shoreward side of the sandbar. The undertow currents erode the sandbar crest and deposit sediments offshore. Gravity-driven transport favors sandbar diffusion. Acceleration skewness accounts for most of the bed level changes over the sandbar.

4.2 | Individual optimization and resulting model skill

It was observed that batch and individual optimizations yield different results for the model coefficients and model skill in Figure 4. Similar to the training and validation cases, individual optimization of calibration coefficients was performed on the 21 test cases. Figure 11 (a) presents the predictive skill for all 101 cases obtained using individually optimized coefficients. As expected, an improvement in model skill is observed compared to batch-optimized results (individually optimized $\bar{BSS} = 0.86$, batch optimized $\bar{BSS} = 0.66$). The spread in the parameter values obtained from individual optimization is also provided in Figure 11(b). A considerable variation in coefficient values is observed, especially for k_v,k_c, and k_d. However, the medians of individually optimized coefficient distributions are similar to the values of batch-optimized coefficients.

4.3 | Comparison of the proposed model with existing morphological models

The proposed model skill is compared with two state-of-the-art morphodynamic models, Unibest-TC and XBeach, for the onshore sandbar migration cases used in this study.

4.3.1 | Comparison with Unibest-TC

The processes-based wave averaged morphodynamics model Unibest-TC (Ruessink et al., 2007) was developed to model cross-shore sediment dynamics and morphological changes. In previous studies, Unibest-TC has successfully captured sandbar migrations (e.g., Pape et al., 2010; Ruessink et al., 2007; Walstra et al., 2012). Bedload transport calculated in Unibest-TC accounts for the near-bed intra-wave orbital velocities, infragravity motion, and currents (Ruessink et al., 2007). It is noted that the short-wave intra-wave

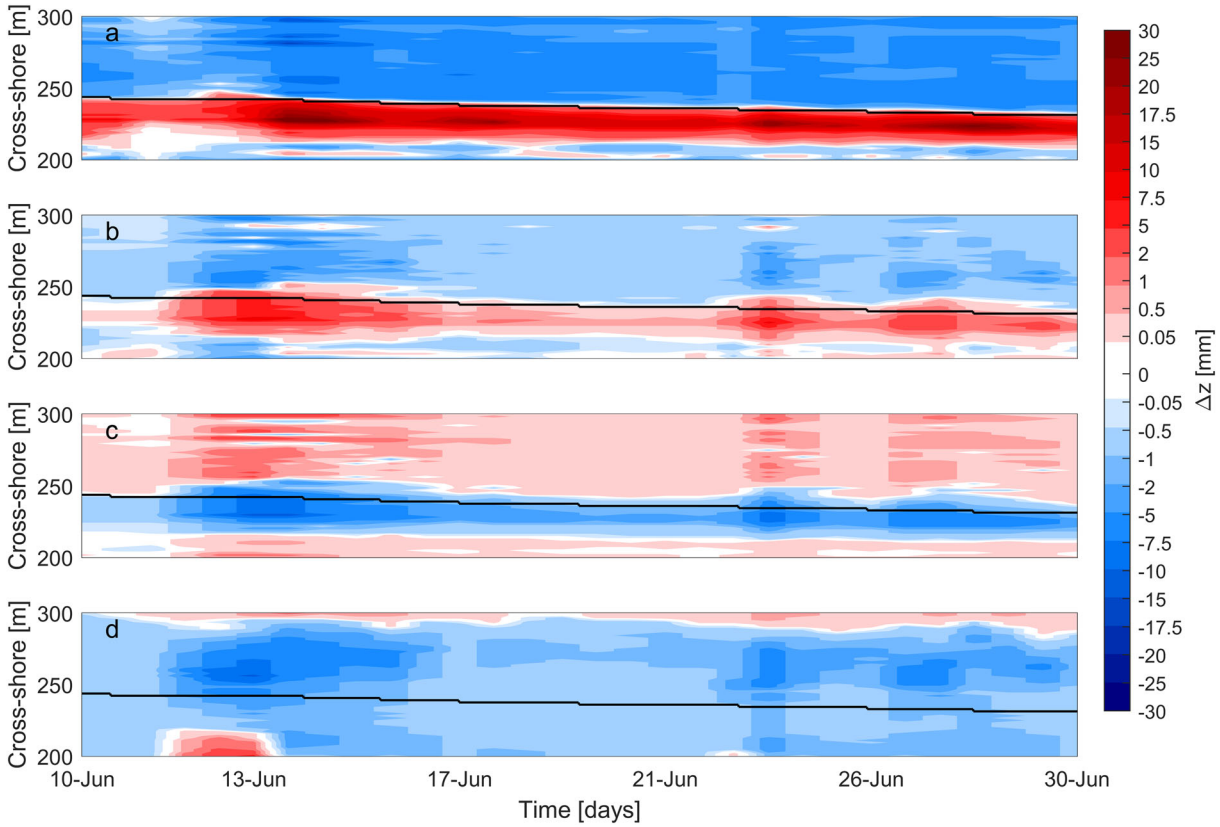

FIGURE 10 Bottom changes in the surroundings of the sandbar over time for case 02 ($\bar{H}_s = 0.58\,m, \bar{T}_p = 8.6\,s$) due to (a) S_{ask}, (b) S_{vsk}, (c) S_c, and (d) S_D respectively. The solid black line indicates the sandbar crest location. The cross-shore distance is measured from the shoreline

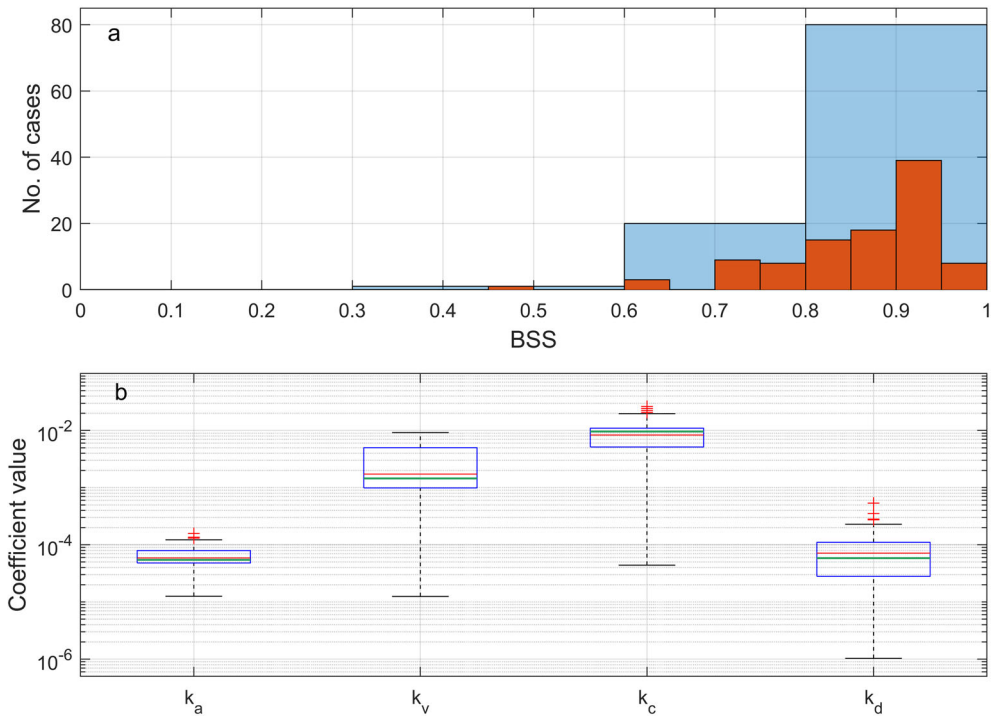

FIGURE 11 (a) BSS results for all cases using individually optimized sediment transport coefficients. Blue bins represent the BSS classification: fair, good, and excellent. The red bins provide the BSS at a bin resolution of 0.05. (b) Box and whisker plots for model coefficients obtained from individual optimization. Outliers are defined as values greater than or less than Q_3+1.5 × IQR, Q_1 − 1.5 × IQR where $Q_1$and Q_3 are the first and the third quartile of the data, respectively, and IQR is the interquartile range. The green line in each boxplot indicates the batch optimized model coefficients

velocity approximation contains non-zero velocity skewness but zero acceleration skewness. The model is described in detail in Ruessink et al. (2007).

The prediction skill of the proposed approach was compared with that of Unibest-TC. Unibest-TC contains several parameters that need calibration. Previous studies that used the model to predict sandbar migrations found that the model results are sensitive to the following parameters; scaling for offshore directed transport due to infragravity currents (c_r), current related roughness (k_c), tangent of the angle of repose (tanϕ), and scale factor for the vertical eddy viscosity distribution function in the undertow model (α_w). Bedload transport is affected by c_r and tanϕ. The c_r changes the magnitude of the offshore directed transport due to infragravity currents, and tanϕ accounts for the effect of bed slope on sediment transport. The k_c and α_w influence the suspended sediment transport. The k_c alters the reference height in the computation of suspended sediment transport, thus influencing its magnitude. The α_w affects the variation of cross-shore velocities in the vertical, thus changing the advection velocity of the suspended sediments.

To compare the skill of Unibest-TC with the presented model, Unibest-TC was calibrated with the same training cases as earlier. The optimal values for the parameters were found by minimizing the objective function, J_{UN}:

$$J_{UN}(c_r, k_c, \tan\phi, \alpha_w) = \frac{\sum_{i=1}^{N}(1-\mathrm{BSS}(i))^2}{N}. \quad (15)$$

Optimum calibration coefficients were derived using the same optimization procedure described earlier. Initializations for the optimization were set by performing a coarse grid search in the parameter space used in previous studies. From the training data, it was found that the optimal coefficient values for c_r, k_c,tanϕ and α_w were 0.110, 0.036, 0.506 and 0.106 respectively. These values are comparable with the values obtained in previous studies (Ruessink et al., 2007).

The derived calibration factors were then used to predict the sandbar migration of all cases. All other parameters of Unibest-TC were kept as default. The default values of the parameters are given in Table 2. The BSS was calculated for each case in the same profile extent and grid as in the presented model. Unibest-TC was able to achieve an average BSS of 0.58.

Figure 12 provides a comparison of the BSS between the presented model and Unibest-TC. Out of the total 101 cases, 35 cases have a similar modeling skill for both models ($|\mathrm{BSS}_{\mathrm{Unibest-TC}} - \mathrm{BSS}_{\mathrm{our\ model}}| < 0.1$). Our model surpasses the skill of Unibest-TC for 40 cases, while Unibest-TC was able to outperform our model for 26 cases. Furthermore, Unibest-TC performed poorly (BSS < 0.3) in 15 cases, while our model performed poorly for six cases.

Individual optimization (Equation 15, $N = 1$) of Unibest-TC for all 101 cases was also performed, and Figure 13(a) presents the BSS values obtained from this process. The individual optimization yields better results ($\bar{BSS} = 0.80$) compared to the batch optimized (Figure 12c) outcomes ($\bar{BSS} = 0.58$). Figure 13(b) gives the spread in calibration coefficients for individual optimization. A similar variation in the coefficient values to that of the proposed model is observed for Unibest-TC.

4.3.2 | Comparison with XBeach

XBeach (Roelvink et al., 2010) is a widely-used morphodynamic model initially developed to simulate erosional conditions. However, as pointed out by Roelvink and Costas (2019), important functionalities to simulate onshore transport have also been implemented over the years. Recent studies have used XBeach to simulate beach recovery conditions (e.g., Cohn et al., 2019; Daly et al., 2017; Pender & Karunarathna, 2013). Since XBeach is a widely used morphodynamic model, the proposed model was compared with XBeach.

XBeach accounts for wave asymmetry and skewness by modifying the sediment advection velocity. The short-wave skewness and asymmetry are parametrized based on empirical equations, which are modified by the calibration parameters fac_{sk} and fac_{As}, respectively. Previous studies have observed that XBeach results are sensitive to these parameters (Nederhoff et al., 2015; Vousdoukas et al., 2012).

TABLE 2 Important default parameters of XBeach and Unibest-TC that were not calibrated in the optimization procedure

	Parameter	Description	Default value
XBeach	*fw*	Short-wave friction coefficient	0.0
	gamma	Breaker index in the wave dissipation model	0.78
	Alpha	Wave dissipation coefficient	1.0
	wetslp	Critical avalanching slope underwater	0.3
	Bedfriction	Bed friction formula and coefficient	Chezy,55
Unibest-TC	*rw*	Wave related roughness	0.002
	gamma	Breaking parameter	"0"(Stive & Battjes, 1984)
	alphac	Wave breaking parameter	1.0
	rkval	Friction factor for mean currents	0.01
	fwee	Friction factor for bottom friction	0.01

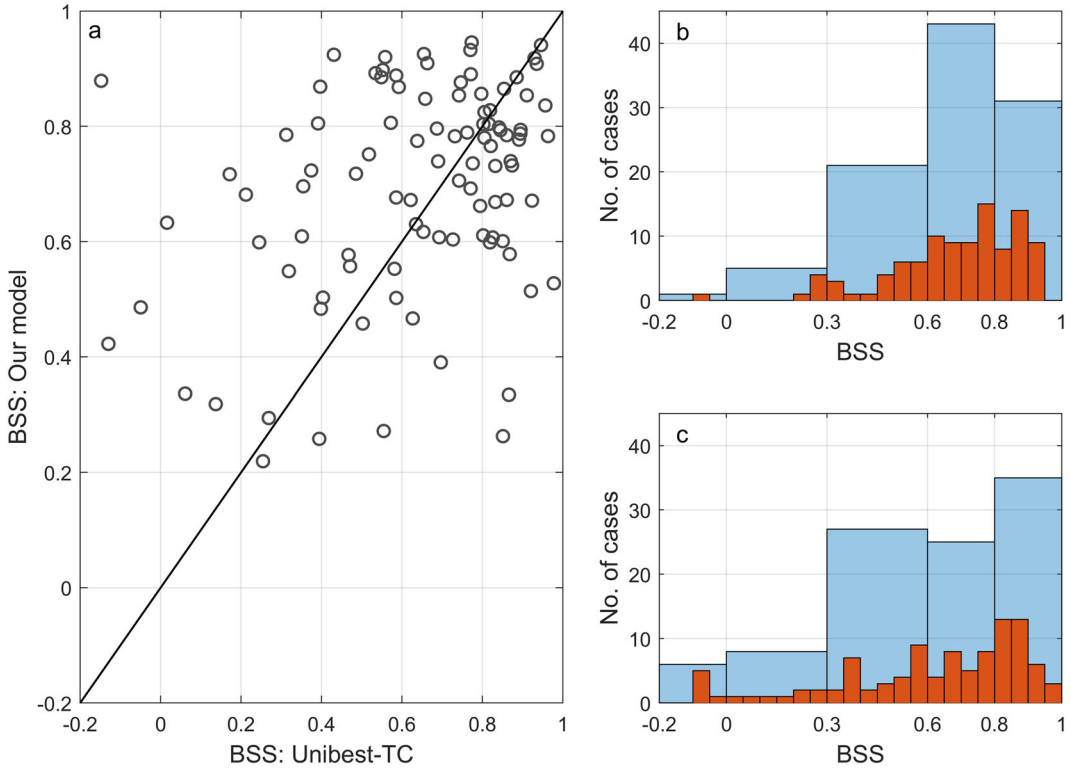

FIGURE 12 (a) Comparison of BSS between Unibest-TC and our model. The solid black line shows the $BSS_{Unibest-TC} = BSS_{our\ model}$. (b) BSS results for all cases using the presented model. (c) BSS results for all cases using Unibest-TC. In the histograms, blue bins represent the BSS classification: no-skill, poor, fair, good, and excellent. The red bins provide the BSS at a bin resolution of 0.05. Note in the histogram, BSS < −0.1 are lumped as BSS = −0.1 for easier representation

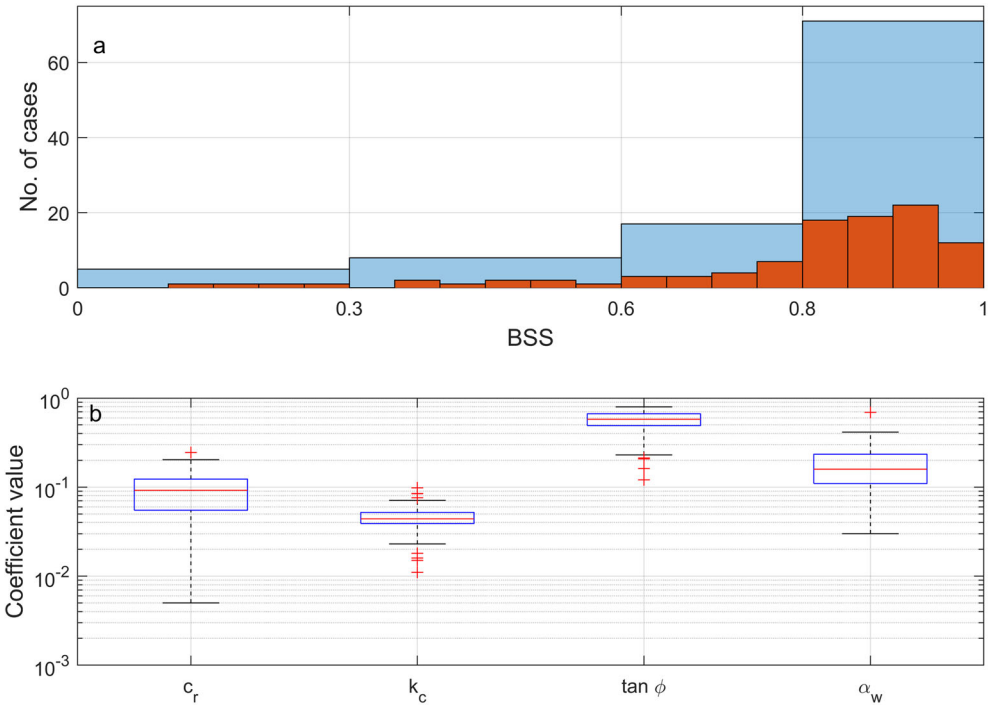

FIGURE 13 (a) BSS results for all cases using individually optimized c_r, k_c, tanø, and α_w. Blue bins represent the BSS classification: no-skill, poor, fair, good, and excellent. The red bins provide the BSS at a bin resolution of 0.05. (b) Box and whisker plots for model coefficients obtained from individual optimization. Outliers are defined as values greater than or less than Q_3+1.5 × IQR, Q_1 − 1.5 × IQR where $Q_1$and Q_3 are the first and the third quartile of the data, respectively, and IQR is the interquartile range

Furthermore, Bugajny et al. (2013) identified fac_{sk} and fac_{As} to affect the XBeach results the most. Therefore, these two coefficients are calibrated in this work.

To be consistent with the calibration of the proposed model (which calibrates four coefficients), the wave roller and the bed slope effect on sediment transport are also calibrated in XBeach. The wave

roller acts as temporary storage of momentum, and subsequent roller energy dissipation occurs based on the wave-front slope. The breaker slope coefficient (β) was used as a calibration coefficient. Roller energy dissipation affects the location of maximum wave breaking, sediment concentration, and undertow (Zimmermann et al., 2015). The bed slope can influence sediment transport by changing the magnitude and direction of transport (Walstra et al., 2007). XBeach accounts for the effect of bed slope by adjusting the transport rates based on the local bed slope, water depth, velocity, and sediment concentration. The fac_{sl} which influence the magnitude of the adjustment to the sediment transport rate is calibrated in this study. More details on the XBeach formulation can be found on Roelvink et al. (2010).

Optimum calibration coefficients of XBeach were derived similarly to that of Unibest-TC and the proposed model. From the training data, it was found that the best coefficient values for fac_{sk}, fac_{As}, β, and fac_{sl} were 0.31, 0.21, 0.12 and 0.08 respectively. The optimum calibration factors were then used in predicting all the cases. All other parameters of XBeach were kept as default and are given in Table 2. The BSS was calculated for each case in the same profile extent and grid as our model. XBeach was able to achieve an average BSS of 0.48.

Figure 14 provides a comparison of the results between the presented model and XBeach. Out of the total 101 cases, 21 cases have a similar modeling skill for our model and XBeach ($|BSS_{XBeach} - BSS_{our\ model}| < 0.1$). Our model surpasses the skill of XBeach for 64 cases, while XBeach was able to outperform our model for only 16 cases. Furthermore, XBeach performed poorly (BSS < 0.3) in 26 cases.

From the three models, calibrated XBeach showed the lowest skill ($\bar{BSS} = 0.48$) for the onshore sandbar bar migration cases. Unibest-TC was able to archive a higher skill compared to XBeach ($\bar{BSS} = 0.58$). The proposed model was able to outperform both morphodynamic models with an average skill score of $\bar{BSS} = 0.66$.

4.4 | Comparison of sediment transport estimations with observations

The three models (proposed model, Unibest-TC, and XBeach) use different methods to calculate sediment transport. The accuracy of net sediment transport estimations was assessed by comparing them with flume observations. The sandBAR SEDiment (BARSED) flume experiments (Mieras et al., 2017) were used to compare the model results. A fixed, barred cross-shore profile that represents a Duck, NC beach was used in the flume experiments. A sediment pit was installed at the crest of the sandbar in place of the immovable bed. Velocity and concentration measurements were conducted at the crest of the sandbar. Wave cases were simulated using monochromatic waves, consisting of incident wave height ranging from 0.4 m to 0.6 m and wave periods of 5 s to 9 s. The experimental method is described in

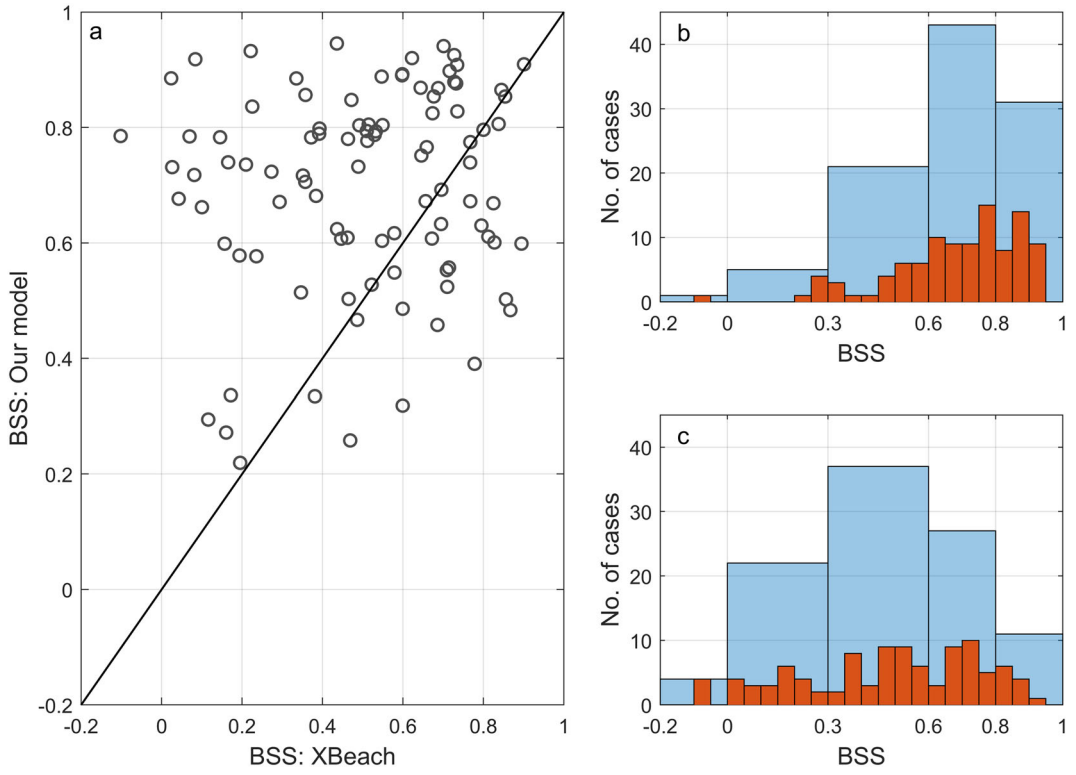

FIGURE 14 (a) Comparison of BSS between XBeach and our model. The solid black line shows the $BSS_{XBeach} = BSS_{our\ model}$. (b) BSS results for all cases using our model. (c) BSS results for all cases using XBeach. In the histograms, blue bins represent the BSS classification: no-skill, poor, fair, good, and excellent. The red bins provide the BSS at a bin resolution of 0.05. Note in the histogram, BSS < 0 are lumped as BSS = −0.1 for easier representation

detail in Mieras et al. (2017, 2019). Mieras et al. (2019) found that bedload transport was the dominant mode of transport for most wave cases simulated in the flume.

The measured phase-average and wave-average net bedload transports in the wave cases were compared with the estimations from the three models. The measured near-bed free stream velocity (u_∞) was used in all three models to estimate bedload transport. For a prescribed velocity signal, only the coefficients in sediment transport remain to be calibrated from the chosen parameters. Since the BARSED experiments were performed on a flat sediment pit on the sandbar crest, $\frac{dz_b}{dx} = 0$, and only one calibration coefficient for Unibest-TC (k_c) was left to calibrate. Two free coefficients were left for XBeach (fac_{sk} and fac_{As}), and three for the proposed model (k_a,k_v,k_c). To have the same degrees of freedom for all models, two coefficients for each model were calibrated against measured transport values. Hence, wave related roughness (k_w) is introduced as a calibration coefficient for Unibest-TC. As u_∞ contains both orbital and mean velocities, bedload components of Equations 7 and 8 in the proposed model are combined to reduce two calibration coefficients to one (k'_v). Thus the bedload transport for our model is calculated as:

$$S_{bed} = k_a\left(a_{spike} - \text{sign}(a_{spike})a_{cr}\right) + \frac{k'_v}{(s-1)g\tan(\phi)}\frac{\varepsilon_B}{}\left(< |u_\infty|^2 u_\infty >\right). \quad (16)$$

Figure 15 provides the regression between the measured and estimated net bedload sediment transport fluxes for each model. A clear difference in representing the measured bedload transport is observed between the three models, with the proposed model showing the best estimate, followed by Unibest-TC and XBeach. A similar variation in morphological prediction capacity was seen between the models. The difference in morphological skill between the three models can then be associated with the difference in sediment transport prediction capacity.

4.5 | Model predictions of onshore sandbar migration at other locations

The presented model's prediction skill was assessed by applying it at two other sites: the large flume experiment, LIP (Roelvink & Reniers, 1995), and field measurements carried out at Tairua beach, New Zealand (van Maanen et al., 2008).

4.5.1 | LIP experiment

LIP experiments were performed in 1993 at the Delft Hydraulics' Delta flume to understand the hydrodynamics and sediment transport in barred beach profiles. An onshore sandbar migration was observed in the LIP-1C case. Irregular waves with a significant wave height of 0.58 m and a peak wave period of 8 s forced the initial barred cross-shore profile (dashed line in Figure 16) of the LIP-1C test for 13 h. The mean water level was maintained at a constant height of 4.1 m. Details on the experiment can be found in Roelvink and Reniers (1995).

The model parameters were calibrated using the bed level measured at 10 h (not shown here). The obtained parameters are presented in Table 3. Figure 16 provides the observed and the predicted bed level after 13 h. The model was able to capture the sandbar movement with a BSS of 0.56.

4.5.2 | Tairua beach New Zealand

An onshore sandbar migration event was observed at Tariua beach for four days in 2001. The measured offshore wave height, period, and water level are presented in Figure 17(a–c). For our study, the measured data at the site was obtained by digitizing the figures presented

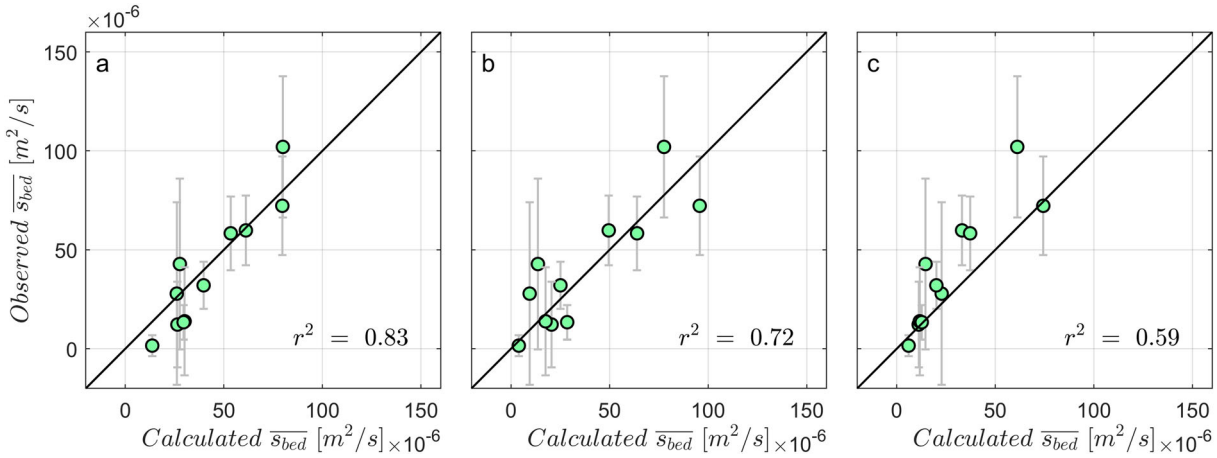

FIGURE 15 Calculated and measured net bedload transport for waves cases in BARSED flume experiments. Bedload transport calculated using (a) the proposed model ($k_a = 2.46 \times 10^{-5}$,$k'_v = 1.94 \times 10^{-2}$), (b) Unibest-TC ($k_c = 0.054$,$k_w = 0.0014$) and (c) XBeach ($fac_{sk} = 4.35$,$fac_{As} = 3.61$). The gray error bars represent one standard deviation from the mean sediment transport rate. The solid black line represents the best fit line for the data points forced through the origin and gradient of one. The r^2provides the correlation between the measured and the calculated values

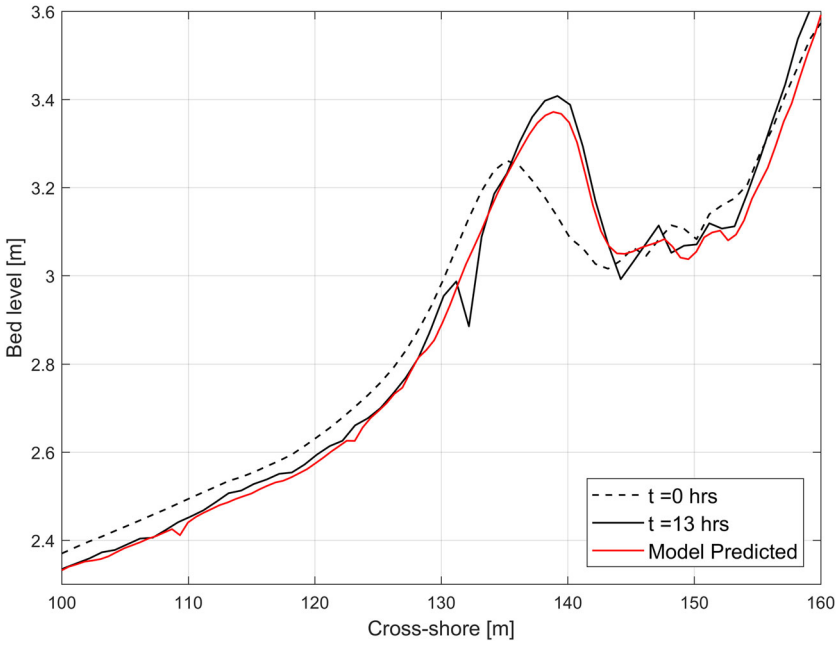

FIGURE 16 Model predictions of onshore sandbar migrations in the LIP-1C flume experiments. The black dashed line refers to the observed initial bed level. The black and red solid lines indicate the final observed and modeled bed level, respectively. The cross-shore distance is measured from the shoreline

TABLE 3 Optimized sediment transport coefficients for the three locations

Location	k_a	k_v	k_c	k_d
Duck, NC	5.46×10^{-5}	1.45×10^{-3}	9.61×10^{-3}	5.85×10^{-5}
LIP-1C	5.74×10^{-6}	1.16×10^{-2}	9.59×10^{-4}	2.46×10^{-6}
Tairua beach	1.14×10^{-4}	1.54×10^{-4}	2.45×10^{-4}	1.77×10^{-5}

by van Maanen et al. (2008). More details on the observations can be found in van Maanen et al. (2008).

The sandbar migration was predicted using the initial measured cross-shore profile (t = 0 days) and measured hydrodynamic conditions. The model coefficients were calibrated using the profile measurements done on t = 1.06 days. The calibration coefficients are presented in Table 3. The sandbar at this site is located at a shallow depth. To avoid hydrodynamic and sediment transport fluxes at very shallow depths, they were not calculated for depths < 0.25 m. A similar approach has been used in van Maanen et al. (2008) to compute the sandbar migration in their study.

Figure 17(d–f) presents the predicted bed variation with time. A BSS of 0.77, 0.71, and 0.73 was obtained for the simulations at t = 1.06 days, t = 1.99 days, and t = 2.79 days respectively. The model shows reasonable skill in predicting the change in sandbar morphology. However, an overprediction of sandbar height and underprediction of cross-shore migration is observed for t = 1.99 days and t = 2.79 days. The shallow water depths encountered over the sandbar during low tidal conditions may be a reason for the deviation between the predicted and observed sandbar migration. Table 3 presents the comparison of the calibrated model coefficients at the three locations. Inter-site variation of the coefficient values can be observed for all four parameters.

The changes in the parameter values could be due to differences in site conditions. During optimization, the parameter values will change between locations to compensate for these variations not captured in the model. For example, the grain size is different between the three sites. At Duck, NC and LIP-1C, the median grain size is ≈0.2 mm while the median grain size at Tairua beach is much coarser (0.6 mm). While the sediment fall velocity was calculated based on the grain size using the method proposed by Ahrens (2000), the effect of grain size on parameters a_{cr}, $\tan\phi$, ε_B, ε_S are not considered in this study and were kept constant for all three sites. The influence of grain size on these parameters can be a reason for the variation observed in the calibrated parameter values between the sites and deserves future investigation.

4.6 | Simulating an onshore–offshore sandbar migration

An onshore–offshore sandbar migration event was observed during September 24 and October 4 in the Duck94 field campaign (Figure 18). The event comprised of an onshore migration in the first six days and an offshore migration under energetic wave conditions in the final four days. More information on the observations can be found in Ruessink et al. (2007).

The proposed model is used to simulate the sandbar behavior, starting from the profile survey on September 24. It should be noted that the two onshore sandbar migration cases in this event were not included in the calibration and testing dataset used in the previous sections. The sediment transport coefficients were set to the

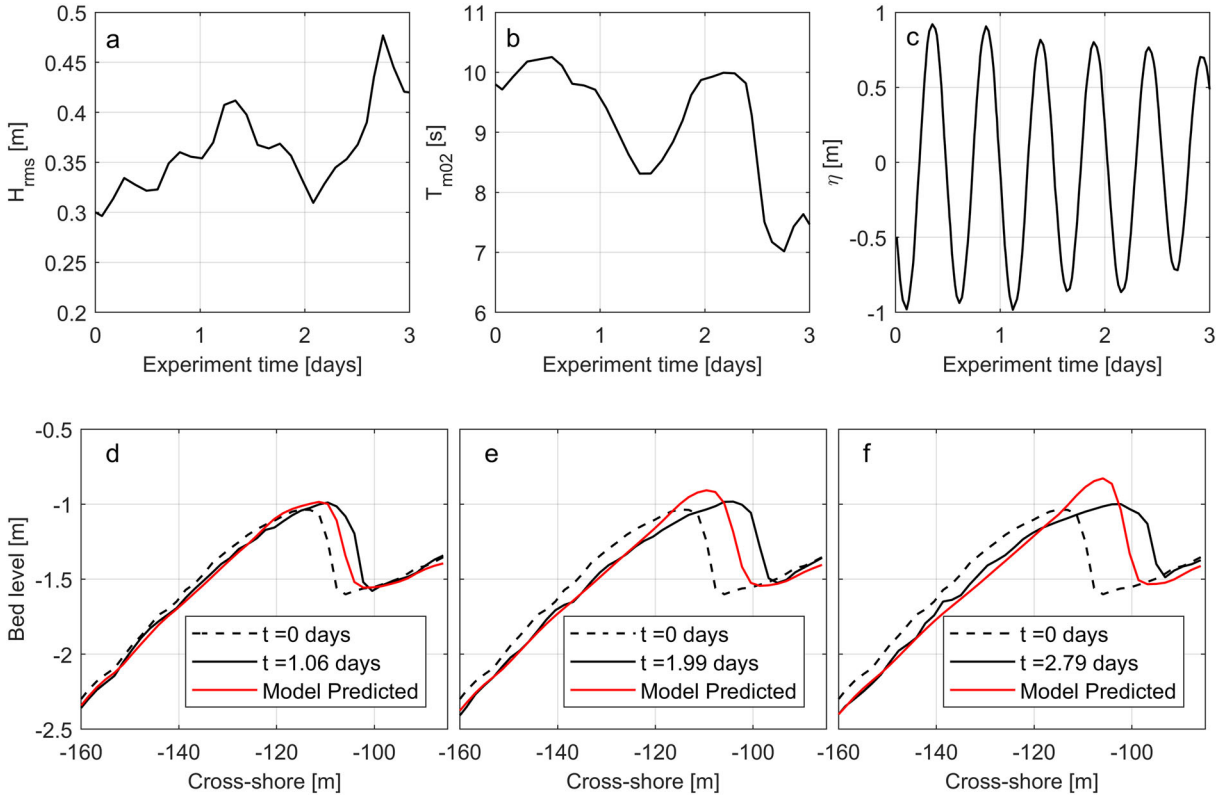

FIGURE 17 (a–c) Measured offshore wave height, period, and the water level. (d–f) Model predictions and the observed sandbar migration at Tairua beach, New Zealand at t = 1.06, t = 1.99, and t = 2.79 days, respectively. The black dashed line refers to the observed initial bed level. The black and red solid lines indicate the final observed and modeled bed level, respectively. The cross-shore distance is measured from the shoreline

same values ($cof_{set\ 1}$) found in section 3.2 ($k_a = 5.46 \times 10^{-5}$, $k_v = 1.45 \times 10^{-3}$, $k_c = 9.61 \times 10^{-3}$, $k_d = 5.85 \times 10^{-5}$). Figure 18(b–d) provides the predicted sandbar displacement. Good agreement between the measured and predicted morphology is observed during the onshore migration of the sandbar (Figure 18b,c), resulting in a BSS of 0.8 and 0.72, respectively. However, the model fails to simulate the offshore sandbar migration during September 30 and October 4 (BSS = −0.67) using the same transport coefficients (Figure 18d, red line). To model the offshore sandbar migration, a different combination of parameters is required such that the onshore sediment transport rate is reduced, and offshore transport is increased. Figure 18 (d) (blue line) provides the offshore sandbar migration predicted from September 30 and October 4. The model coefficients used for the offshore migration ($cof_{set\ 2}$) are k_a=3.82×10^{-6}, k_v=1.96×10^{-3}, k_c=2.85×10^{-1} and $k_d = 7.61 \times 10^{-5}$. By employing the new parameters, the model can successfully predict the offshore sandbar migration (BSS = 0.76). It is observed that the new values of k_a and k_c are respectively an order of magnitude smaller and larger than the batch optimized values. The change in transport coefficients results in a reduction of acceleration induced onshore transport and an increase of undertow driven offshore transport.

Previous studies have also used different coefficients to simulate accretional and erosional conditions (e.g., Cohn et al., 2019; Pender & Karunarathna, 2013; Plant et al., 2004). However, requiring different parameters to model the offshore sandbar migration indicates that the proposed approach lacks physical processes needed to accurately capture offshore sandbar migration.

While the presented model accounts for offshore transport due to undertow currents, other processes that can be important in offshore transport, such as infragravity currents (Aagaard & Greenwood, 2008; Bertin et al., 2018), wave roller propagation (Ribas et al., 2011), vertical variation of undertow currents (Lentz et al., 2008), and lag effects in suspended transport (Kim et al., 2017) are currently unresolved in the model. The optimization procedure likely changes coefficients for the offshore sandbar migration case to compensate for these unresolved processes. Further considerations on how the model could be improved to capture offshore sandbar migrations are provided in section 4.8.

4.7 | Model prediction for double sandbar cases

The model was used to predict the morphological evolution of double sandbars observed at Duck, NC. A set of 10 cases not included previously were simulated using the same calibration coefficients obtained in section 3.2. The bed profiles of the double bar cases contained a shallow and a deeper sandbar that was located at an average depth of 1.4 m and 2.5 m, respectively. In the simulated cases, both sandbars

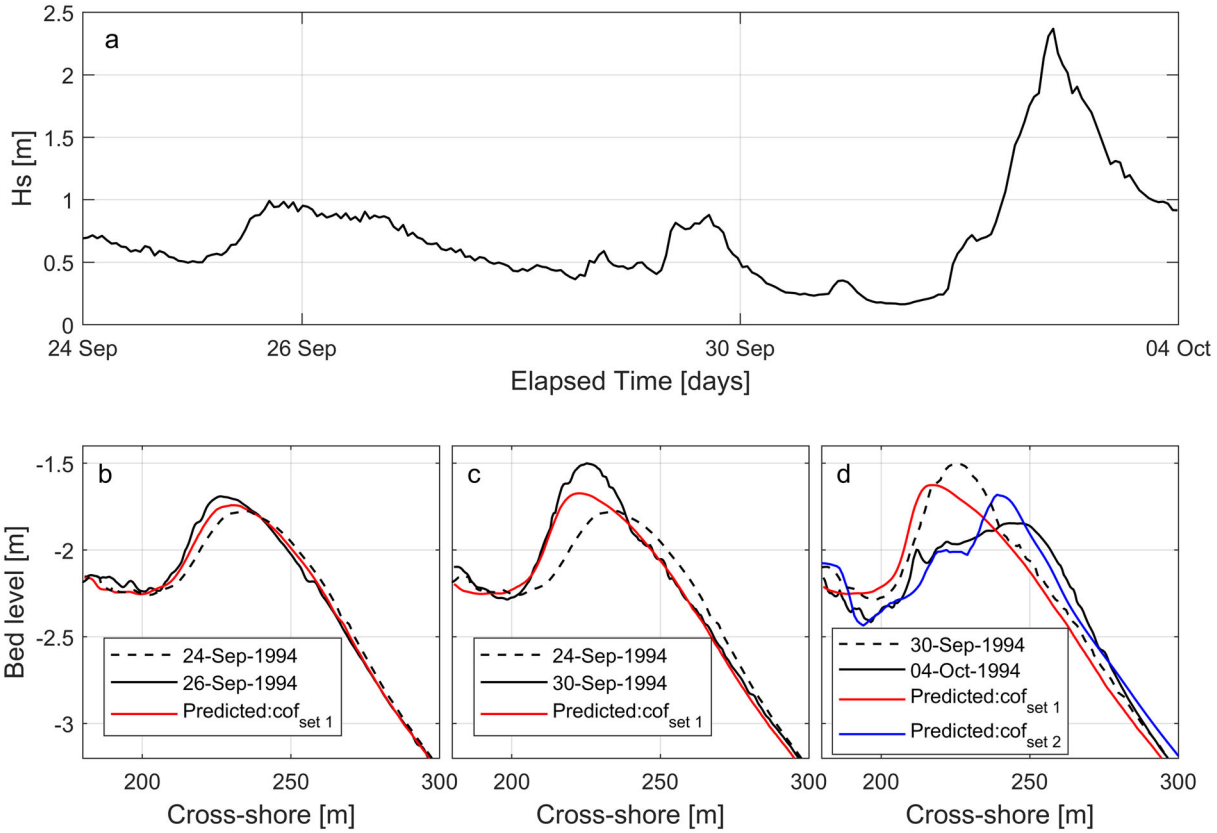

FIGURE 18 Onshore–offshore sandbar migration event observed in Duck, NC, from September 24 to October 4, 1994. (a) Measured significant wave height. (b–d) Measured and model-predicted bed level. The red line provides the predicted sandbar morphology using the model coefficient set 1 (cof_{set1}) : $k_a = 5.46 \times 10^{-5}$, $k_v = 1.45 \times 10^{-3}$, $k_c = 9.61 \times 10^{-3}$, $k_d = 5.85 \times 10^{-5}$ and the blue line shows the predicted sandbar morphology using the model coefficient set 2 (cof_{set2}): k_a=3.82×10^{-6}, k_v= 1.96×10^{-3}, k_c=2.85 ×10^{-1} and k_d=7.61 ×10^{-5}. The cross-shore distance is measured from the shoreline

moved onshore. The shallower sandbars had larger displacements than the deeper ones, where the latter only moved by 40% of the shallow sandbar displacement.

Figure 19 presents the measured and predicted bed evolution for a subset of cases. While the model can capture both bar migrations ($\bar{BSS}$ = 0.57), the shallower sandbar migration is better represented compared to the deeper bar. The lesser reproduction of the deeper sandbar movement could be because the model coefficients were trained only on single sandbar cases, thus focusing the model strength more on the shallower sandbar.

4.8 | Limitations of the model and further considerations

Our model was able to make good predictions for most of the onshore sandbar migration events. Nevertheless, in some cases, the model skill was not satisfactory.

The velocity reconstruction by Elfrink et al. (2006) is based on a wide range of wave conditions. However, the wave conditions are not evenly distributed over the parameter space (wave height, wave period, etc.). Hence, the reconstruction may not be trained well when there are only a few conditions available. The reconstruction in such situations can lead to incorrect velocity signals and thus to erroneous model predictions. The majority of wave data used in Elfrink et al. (2006) model lies in the ranges of $H/h < 0.4$ and $L/h < 16$ where H is the wave height, L is the wave length. Using model output, H/h, L/h and duration of occurrence of each wave condition over the sandbar were calculated for all cases. The $T_{\%out}$ is defined as the average percentage duration of wave condition occurring outside the said data range of Elfrink et al. (2006). A lower $T_{\%out}$ means that the majority of the wave climate encountered in the case is within the data coverage. For all cases $T_{\%out}$ was 36.7% with a standard deviation of 20.3%. For the 10 highest performing cases, wave conditions outside the data range was 36.1% and for the 10 lowest performing cases, $T_{\%out}$ was 52.5%. Hence, it is evident that cases which encounter lower percentage of wave conditions outside the data coverage performs better than the ones that encounter higher percentage of wave conditions outside the data coverage. Extending the range of applicability of the intra-wave orbital reconstruction method of Elfrink et al. (2006) by including more wave data can improve the orbital velocity reconstruction and the model results.

As discussed in section 4.6, some hydrodynamic processes that are particularly important in offshore migration of sandbars are

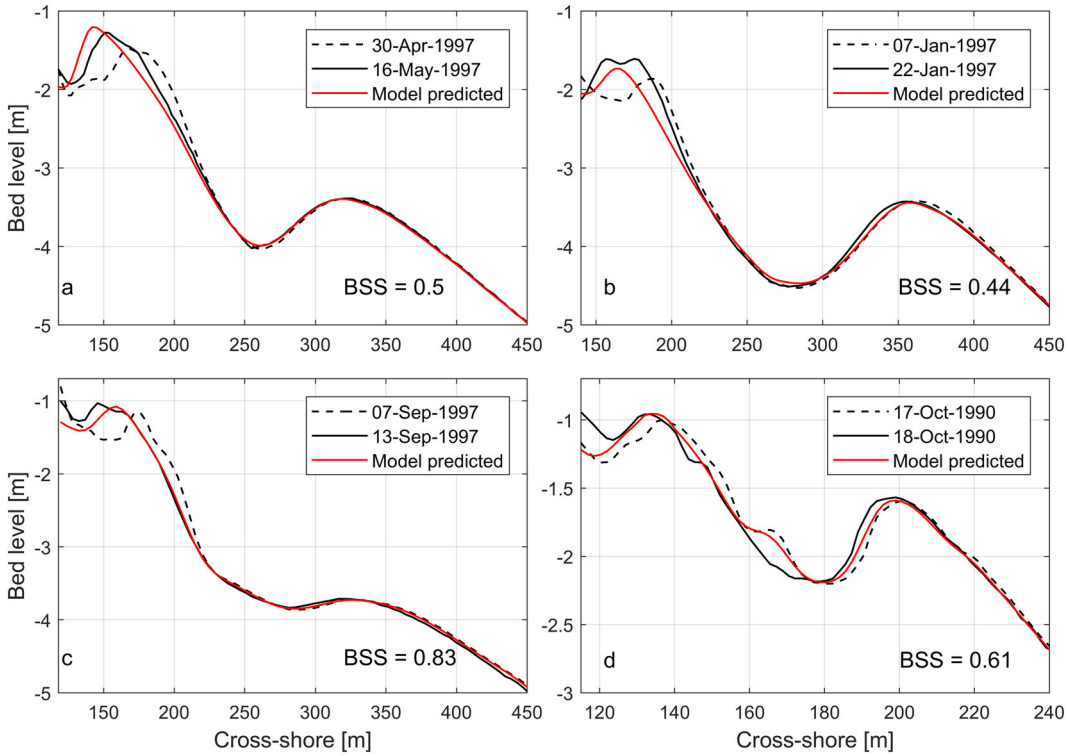

FIGURE 19 (a–d) Model predicted sandbar morphology for four double bar cases. The black dashed line refers to the observed initial bed level. The black and red solid lines indicate the final observed and modeled bed level, respectively. The cross-shore distance is measured from the shoreline

currently unresolved in the proposed approach. Also, the current model does not account for longshore processes, which can influence sandbar morphology.

BSS is used to calibrate and measure the prediction skill of sandbar migrations in the study. While BSS is a competent indicator to quantify model skill, certain drawbacks have also been identified (Bosboom et al., 2014). BSS tends to favor cases that underestimate the variance in bed level change. Model predictions in this study did not result in superfluous BSS rankings compared to visual assessment. However, it was observed that the cases with an underpredicted migration resulted in a lower variance in bed level change compared to observed values. Conversely, cases with an overpredicted migration have a larger variance in bed level change.

While underpredicted/overpredicted cases visually showed a similar mishandling of sandbar prediction, the cases with an underpredicted migration resulted in a higher BSS ranking compared to the overpredicted cases. Since the model parameters were derived using many cases, a general underprediction of sandbar migration rate was not observed.

The area of interest in the current study is the vicinity of the sandbar. Energetic type transport formulations used to calculate the sediment transport fluxes may not be suitable to estimate the bed level changes observed in the swash zone (Masselink et al., 2009) and require other formulations to represent these processes.

As future work, the presented model is being included within the XBeach framework. Appropriate merging of processes discussed in this study with physics that are already implemented in XBeach (such as: infragravity waves, wave roller, vertical profile of undertow, swash processes) will enable predictions of the full extent of the cross-shore transect under erosive and accretional conditions.

According to the classification of onshore sandbar migration modes by Vidal-Ruiz and Ruiz de Alegría-Arzaburu (2019, 2020), the cases used in this study can be generally classified as mode I (section 2.4). The other identified modes (modes II–IV) consist of compounds of onshore and offshore sandbar migrations. As a future study, a modified XBeach model (with the current model) can be used to assess the predictability of the other observed modes of sandbar migrations.

5 | CONCLUSION

A simplified process-based model to predict onshore sandbar migration is proposed. The model includes sediment transport processes due to wave asymmetry, skewness, mean currents, and bed-slope effects. A velocity reconstruction is incorporated to calculate the sediment transport induced by waves.

A systematic training, validation, and testing procedure were carried out using multiple onshore sandbar migration cases to ensure the model is not overfitting, and it can produce reliable predictions.

The presented approach shows good predictive skills for onshore sandbar migration cases without an *ad hoc* calibration for each

scenario. The model was also able to outperform widely used morphodynamic models (XBeach and Unibest-TC) on the onshore sandbar migration cases used in this study. The higher skill of the proposed model can be associated with the better transport prediction capacity observed for the model.

The model was also tested using onshore migration cases at different locations. While the model performed well at the different sites, optimum parameter values varied between the locations. The changes in the parameter values could be due to differences in site conditions that were not included in the model.

Further improvements are required for the presented model to simulate offshore sandbar migration.

ACKNOWLEDGEMENTS

The authors thank Spicer Bak and Patrick Dickhudt (Field Research Facility in Duck, NC) for answering questions on data collected at the site. The authors also thank Deltares for providing the Unibest-TC software and Dano Roelvink (Deltares/IHE Delft, The Netherlands) for providing the LIP data. The authors also acknowledge the two anonymous reviewers for their useful comments on this manuscript.

CONFLICT OF INTEREST

The authors declare that they have no conflicts of interest.

DATA AVAILABILITY STATEMENT

The Duck, NC data used in this study is available at http://www.frf.usace.army.mil/.

ORCID

Viyaktha Hithaishi Hewageegana https://orcid.org/0000-0002-4433-6011

Alberto Canestrelli https://orcid.org/0000-0003-3264-3169

REFERENCES

Aagaard, T. & Greenwood, B. (2008) Infragravity wave contribution to surf zone sediment transport - the role of advection. *Marine Geology*, 251 (1-2), 1–14. https://doi.org/10.1016/j.margeo.2008.01.017

Abreu, T., Silva, P.A., Sancho, F. & Temperville, A. (2010) Analytical approximate wave form for asymmetric waves. *Coastal Engineering*, 57(7), 656–667. https://doi.org/10.1016/j.coastaleng.2010.02.005

Ahrens, J.P. (2000) A fall-velocity equation. *Journal of Waterway, Port, Coastal, and Ocean Engineering*, 126, 99–102. https://doi.org/10.1061/(ASCE)0733-950X(2000)126:2(99)

Bailard, J.A. (1982) An energetics total load sediment transport model for a plane sloping beach. *Journal of Geophysical Research, Oceans*, 86, 10938–10954.

Baldock, T.E., Holmes, P., Bunker, S. & Van Weert, P. (1998) Cross-shore hydrodynamics within an unsaturated surf zone. *Coastal Engineering*, 34(3-4), 173–196. https://doi.org/10.1016/S0378-3839(98)00017-9

Battjes, J.A. & Janssen, J.P.F.M. (1978) Energy loss and set-up due to breaking of random waves. *Coastal Engineering*, 1978(32), 569–587.

Bertin, X., de Bakker, A., van Dongeren, A., Coco, G., André, G., Ardhuin, F. *et al.* (2018) Infragravity waves: From driving mechanisms to impacts. *Earth-Science Reviews*, 177, 774–799. https://doi.org/10.1016/j.earscirev.2018.01.002

Boechat Albernaz, M., Ruessink, G., Jagers, H.R. & Kleinhans, M.G. (2019) Effects of wave orbital velocity parameterization on nearshore sediment transport and decadal & morphodynamics. *Journal of Marine Science and Engineering*, 7(6), 188. https://doi.org/10.3390/jmse7060188

Bosboom, J., Reniers, A.J.H.M. & Luijendijk, A.P. (2014) On the perception of morphodynamic model skill. *Coastal Engineering*, 94, 112–125. https://doi.org/10.1016/j.coastaleng.2014.08.008

Bowen, A. J. (1980) Simple models of nearshore sedimentation; beach profiles and longshore bars. The coastline of Canada, Paper 80-10, 1–11.

Brown, J.A., MacMahan, J.H., Reniers, A.J.H.M. & Thornton, E.B. (2015) Field observations of surf zone–inner shelf exchange on a rip-channeled beach. *Journal of Physical Oceanography*, 45(9), 2339–2355. https://doi.org/10.1175/JPO-D-14-0118.1

Bugajny, N., Furmańczyk, K., Dudzińska-Nowak, J. & Paplińska-Swerpel, B. (2013) Modelling morphological changes of beach and dune induced by storm on the southern Baltic coast using XBeach (case study: Dziwnow spit). *Journal of Coastal Research*, 65, 672–677. https://doi.org/10.2112/si65-114.1

Cohn, N., Hoonhout, B.M., Goldstein, E.B., de Vries, S., Moore, L.J., Vinent, O.D. & Ruggiero, P. (2019) Exploring marine and aeolian controls on coastal foredune growth using a coupled numerical model. *Journal of Marine Science and Engineering*, 7(1), 1–25. https://doi.org/10.3390/jmse7010013

Daly, C., Floc'h, F., Almeida, L.P. & Almar, R. (2017) Modelling accretion at Nha Trang Beach, Vietnam. *Coastal Dynamics*, 170, 1886–1896.

Drake, T.G. & Calantoni, J. (2001) Discrete particle model for sheet flow sediment transport in the nearshore. *Journal of Geophysical Research, Oceans*, 106(C9), 19859–19868. https://doi.org/10.1029/2000JC000611

Dubarbier, B., Castelle, B., Marieu, V. & Ruessink, G. (2015) Process-based modeling of cross-shore sandbar behavior. *Coastal Engineering*, 95, 35–50. https://doi.org/10.1016/j.coastaleng.2014.09.004

Dubarbier, B., Castelle, B., Ruessink, G. & Marieu, V. (2017) Mechanisms controlling the complete accretionary beach state sequence. *Geophysical Research Letters*, 44(11), 5645–5654. https://doi.org/10.1002/2017GL073094

Elfrink, B., Hanes, D.M. & Ruessink, B.G. (2006) Parameterization and simulation of near bed orbital velocities under irregular waves in shallow water. *Coastal Engineering*, 53(11), 915–927. https://doi.org/10.1016/j.coastaleng.2006.06.002

Elgar, S., Gallagher, E.L. & Guza, R.T. (2001) Nearshore sandbar migration. *Journal of Geophysical Research, Oceans*, 106(C6), 11623–11627. https://doi.org/10.1029/2000JC000389

Fernández-Mora, A., Calvete, D., Falqués, A. & De Swart, H.E. (2015) Onshore sandbar migration in the surf zone: New insights into the wave-induced sediment transport mechanisms. *Geophysical Research Letters*, 42(8), 2869–2877. https://doi.org/10.1002/2014GL063004

Gallagher, E., Elgar, S. & Guza, R.T. (1998) Observations of sand bar evolution on a natural beach. *Journal of Geophysical Research, Oceans*, 103 (C2), 3203–3215.

Hajiarabderkani, M., Siadatmousavi, S.M. & Mahmoudof, S.M. (2017) Sandbar migration due to cross-shore sediment transport; a case study of Noshahr coasts, Iran. *International Journal of Maritime Technology*, 7, 29–37. https://doi.org/10.18869/acadpub.ijmt.7.29

Hallermeier, R.J. (1982) Oscillatory bedload transport: Data review and simple formulation. *Continental Shelf Research*, 1(2), 159–190. https://doi.org/10.1016/0278-4343(82)90003-6

Henderson, S.M., Allen, J.S. & Newberger, P.A. (2004) Nearshore sandbar migration predicted by an eddy-diffusive boundary layer model. *Journal of Geophysical Research*, 109(C6), C06024. https://doi.org/10.1029/2003JC002137

Henriquez, M., Reniers, A.J.H.M., Ruessink, B.G. & Stive, M.J.F. (2014) PIV measurements of the bottom boundary layer under nonlinear surface waves. *Coastal Engineering*, 94, 33–46. https://doi.org/10.1016/j.coastaleng.2014.08.004

Hoefel, F. & Elgar, S. (2003) Wave-induced sediment transport and sandbar migration. *Science*, 299(80), 1885–1887. https://doi.org/10.1126/science.1081448

Hsu, T.J., Elgar, S. & Guza, R.T. (2006) Wave-induced sediment transport and onshore sandbar migration. *Coastal Engineering*, 53(10), 817–824. https://doi.org/10.1016/j.coastaleng.2006.04.003

Jacobsen, N.G., Fredsoe, J. & Jensen, J.H. (2014) Formation and development of a breaker bar under regular waves. Part 1: Model description and hydrodynamics. *Coastal Engineering*, 88, 182–193. https://doi.org/10.1016/j.coastaleng.2013.12.008

Kim, D.H., Sanchez-Arcilla, A. & Caceres, I. (2017) Depth-integrated modelling on onshore and offshore sandbar migration: Revision of fall velocity. *Ocean Modelling*, 110, 21–31. https://doi.org/10.1016/j.ocemod.2016.12.011

Lagarias, J.C., Reeds, J.A., Wright, M.H. & Wright, P.E. (1998) Convergence properties of the Nelder–Mead simplex method in low dimensions. *SIAM Journal on Optimization*, 9(1), 112–147. https://doi.org/10.1137/S1052623496303470

Lentz, S.J., Fewings, M., Howd, P., Fredericks, J. & Hathaway, K. (2008) Observations and a model of undertow over the inner continental shelf. *Journal of Physical Oceanography*, 38(11), 2341–2357. https://doi.org/10.1175/2008JPO3986.1

Masselink, G., Russell, P., Turner, I. & Blenkinsopp, C. (2009) Net sediment transport and morphological change in the swash zone of a high-energy sandy beach from swash event to tidal cycle time scales. *Marine Geology*, 267, 18–35. https://doi.org/10.1016/j.margeo.2009.09.003

Mieras, R.S., Puleo, J.A., Anderson, D., Cox, D.T. & Hsu, T. (2017) Large-scale experimental observations of sheet flow on a sandbar under skewed-asymmetric waves. *Journal of Geophysical Research, Oceans*, 122(6), 5022–5045. https://doi.org/10.1002/2016JC012438

Mieras, R.S., Puleo, J.A., Anderson, D., Hsu, T.J., Cox, D.T. & Calantoni, J. (2019) Relative contributions of bed load and suspended load to sediment transport under skewed-asymmetric waves on a sandbar crest. *Journal of Geophysical Research, Oceans*, 124(2), 1294–1321. https://doi.org/10.1029/2018JC014564

Nederhoff, C.M., Lodder, Q.J., Boers, M., den Bieman, J.P. & Miller, J.K. (2015) Modeling the effects of hard structures on dune erosion and overwash, in: The Proceedings of the Coastal Sediments 2015. World Scientific: London. https://doi.org/10.1142/9789814689977_0219

Nielsen, P. (1992) *Coastal bottom boundary layers and sediment transport*, Advanced Series on Ocean Engineering. London: World Scientific. https://doi.org/10.1142/1269

Nielsen, P. (2006) Sheet flow sediment transport under waves with acceleration skewness and boundary layer streaming. *Coastal Engineering*, 53(9), 749–758. https://doi.org/10.1016/j.coastaleng.2006.03.006

Pape, L., Kuriyama, Y. & Ruessink, B.G. (2010) Models and scales for cross-shore sandbar migration. *Journal of Geophysical Research: Earth Surface*, 115(F3), 1–13. https://doi.org/10.1029/2009JF001644

Pender, D. & Karunarathna, H. (2013) A statistical-process based approach for modelling beach profile variability. *Coastal Engineering*, 81, 19–29. https://doi.org/10.1016/j.coastaleng.2013.06.006

Plant, N.G., Holland, K.T., Puleo, J.A. & Gallagher, E.L. (2004) Prediction skill of nearshore profile evolution models. *Journal of Geophysical Research, C: Oceans*, 109(C1), 1–19. https://doi.org/10.1029/2003jc001995

Ribas, F., de Swart, H.E., Calvete, D. & Falqués, A. (2011) Modeling waves, currents and sandbars on natural beaches: The effect of surface rollers. *Journal of Marine Systems*, 88(1), 90–101. https://doi.org/10.1016/j.jmarsys.2011.02.016

Ribberink, J.S. (1998) Bed-load transport for steady flows and unsteady oscillatory flows. *Coastal Engineering*, 34(1-2), 59–82. https://doi.org/10.1016/S0378-3839(98)00013-1

Ribberink, J.S. & Al-Salem, A.A. (1994) Sediment transport in oscillatory boundary layers in cases of rippled beds and sheet flow. *Journal of Geophysical Research*, 99(C6), 12707. https://doi.org/10.1029/94jc00380

Roelvink, D. & Costas, S. (2019) Coupling nearshore and aeolian processes: XBeach and duna process-based models. *Environmental Modelling and Software*, 115, 98–112. https://doi.org/10.1016/j.envsoft.2019.02.010

Roelvink, D. & Reniers, A. (2011) *A Guide To Modeling Coastal Morphology*. London: World Scientific.

Roelvink, J.A. & Reniers, A. (1995) LIP 11D Delta Flume Experiments. WL| Delft Hydraul. Report H2130. http://www.worldcat.org/oclc/212908657

Roelvink, J.A., Reniers, A.J.H.M., Van Dongeren, A., de Vries, J. Lescinski, J. & McCall, R. (2010) XBeach model description and manual. UNESCO-IHE Institute of Water Education. Report June 21, 2010. Delft: IHE Institute of Water Education.

Ruessink, B.G. (2005) Predictive uncertainty of a nearshore bed evolution model. *Continental Shelf Research*, 25(9), 1053–1069. https://doi.org/10.1016/j.csr.2004.12.007

Ruessink, B.G., Kuriyama, Y., Reniers, A.J.H.M., Roelvink, J.A. & Walstra, D.J.R. (2007) Modeling cross-shore sandbar behavior on the timescale of weeks. *Journal of Geophysical Research: Earth Surface*, 112(F3), 1–15. https://doi.org/10.1029/2006JF000730

Ruessink, B.G., Walstra, D.J.R. & Southgate, H.N. (2003) Calibration and verification of a parametric wave model on barred beaches. *Coastal Engineering*, 48(3), 139–149. https://doi.org/10.1016/S0378-3839(03)00023-1

Short, A.D. (1999) *Handbook of Beach and Shoreface Morphodynamics*. Chichester: Wiley.

Simmons, J.A., Harley, M.D., Marshall, L.A., Turner, I.L., Splinter, K.D. & Cox, R.J. (2017) Calibrating and assessing uncertainty in coastal numerical models. *Coastal Engineering*, 125, 28–41. https://doi.org/10.1016/j.coastaleng.2017.04.005

Splinter, K.D., Holman, R.A. & Plant, N.G. (2011) A behavior-oriented dynamic model for sandbar migration and 2DH evolution. *Journal of Geophysical Research, Oceans*, 116(C1), 1–21. https://doi.org/10.1029/2010JC006382

Splinter, K.D., Turner, I.L., Davidson, M.A., Barnard, P., Castelle, B. & Oltman-Shay, J. (2014) A generalized equilibrium model for predicting daily to interannual shoreline response. *Journal of Geophysical Research: Earth Surface*, 119(9), 1936–1958. https://doi.org/10.1002/2014JF003106

Stive, M.J.F. & Battjes, J.A. (1984) A model for offshore sediment transport. In: *Coastal Engineering 1984*. New York, NY: American Society of Civil Engineers, pp. 1420–1436. https://doi.org/10.1061/9780872624382.098.

Thornton, E.B., Humiston, R.T. & Birkemeier, W. (1996) Bar/trough generation on a natural beach. *Journal of Geophysical Research, Oceans*, 101(C5), 12097–12110. https://doi.org/10.1029/96JC00209

Traykovski, P., Hay, A.E., Irish, J.D. & Lynch, J.F. (1999) Geometry, migration, and evolution of wave orbital ripples at LEO-15. *Journal of Geophysical Research, Oceans*, 104(C1), 1505–1524. https://doi.org/10.1029/1998jc900026

van Maanen, B., de Ruiter, P.J., Coco, G., Bryan, K.R. & Ruessink, B.G. (2008) Onshore sandbar migration at Tairua beach (New Zealand): Numerical simulations and field measurements. *Marine Geology*, 253(3-4), 99–106. https://doi.org/10.1016/j.margeo.2008.05.007

van Rijn, L.C., Wasltra, D.J.R., Grasmeijer, B., Sutherland, J., Pan, S. & Sierra, J.P. (2003) The predictability of cross-shore bed evolution of sandy beaches at the time scale of storms and seasons using process-based profile models. *Coastal Engineering*, 47(3), 295–327. https://doi.org/10.1016/S0378-3839(02)00120-5

Vidal-Ruiz, J.A. & Ruiz de Alegría-Arzaburu, A. (2019) Variability of sandbar morphometrics over three seasonal cycles on a single-barred beach. *Geomorphology*, 333, 61–72. https://doi.org/10.1016/j.geomorph.2019.02.034

Vidal-Ruiz, J.A. & Ruiz de Alegría-Arzaburu, A. (2020) Modes of onshore sandbar migration at a single-barred and swell-dominated beach. *Marine Geology*, 426, 106222. https://doi.org/10.1016/j.margeo.2020.106222

Vousdoukas, M.I., Ferreira, Ó., Almeida, L.P. & Pacheco, A. (2012) Toward reliable storm-hazard forecasts: XBeach calibration and its potential application in an operational early-warning system. *Ocean Dynamics*, 62(7), 1001–1015. https://doi.org/10.1007/s10236-012-0544-6

Walstra, D.J.R., Reniers, A.J.H.M., Ranasinghe, R., Roelvink, J.A. & Ruessink, B.G. (2012) On bar growth and decay during interannual net offshore migration. *Coastal Engineering*, 60, 190–200. https://doi.org/10.1016/j.coastaleng.2011.10.002

Walstra, D.J.R., Van Rijn, L.C., Van Ormondt, M., Brière, C. & Talmon, A.M. (2007) The effects of bed slope and wave skewness on sediment transport and morphology, in: Coast. Sediments'07 – Proceedings of the 6th International Symposium on Coastal Engineering and Science of Coastal Sediment Processes. 40926. https://doi.org/10.1061/40926(239)11

Watanabe, A. & Sato, S. (2005) A sheet-flow transport rate formula for asymmetric, forward-leaning waves and currents, in: Coastal Engineering 2004. World Scientific: London; 1703–1714. https://doi.org/10.1142/9789812701916_0136

Wright, L.D., Boon, J.D., Kim, S.C. & List, J.H. (1991) Modes of cross-shore sediment transport on the shoreface of the middle Atlantic bight. *Marine Geology*, 96(1-2), 19–51. https://doi.org/10.1016/0025-3227(91)90200-N

Zijlema, M., Stelling, G. & Smit, P. (2011) SWASH: An operational public domain code for simulating wave fields and rapidly varied flows in coastal waters. *Coastal Engineering*, 58(10), 992–1012. https://doi.org/10.1016/j.coastaleng.2011.05.015

Zimmermann, N., Trouw, K., De Maerschalck, B., Toro, F., Delgado, R., Verwaest, T. & Mostaert, F. (2015) *Scientific support regarding hydrodynamics and sand transport in the coastal zone: Evaluation of XBeach for long term cross-shore modelling. Version 3.0. WL Rapporten, 00_072*. Flanders Hydraulics Research & IMDC: Antwerp, Belgium.

How to cite this article: Hewageegana VH, Canestrelli A. On the predictive skill of morphodynamic models for onshore sandbar migration. *Earth Surf. Process. Landforms*. 2021;1–23. https://doi.org/10.1002/esp.5079